Applied and
Computational
Mathematics
Division

Computing and Applied Mathematics Laboratory

Morphological Instability in Phase-Field Models of Solidification

R. J. Braun, G. B. McFadden, and S. R. Coriell

October 1993

U.S. DEPARTMENT OF COMMERCE
National Institute of Standards and Technology
Gaithersburg, MD 20899

Morphological Instability in Phase-Field Models of Solidification

R.J. Braun
G.B. McFadden
S.R. Coriell

U.S. DEPARTMENT OF COMMERCE
Technology Administration
National Institute of Standards
and Technology
Computing and Applied Mathematics Laboratory
Applied and Computational Mathematics Division
Gaithersburg, MD 20899

Morphological Instability in Phase-Field Models of Solidification

R. J. Braun, G. B. McFadden, and S. R. Coriell

National Institute of Standards and Technology*

Gaithersburg, MD 20899

October 13, 1993

Abstract

We analyze the linear stability of a planar solidification front with sharp-interface and phase-field models in two physical situations: (1) an isothermal system at the melting point in the unperturbed state, and (2) constant-speed growth of a crystal into its hypercooled melt. The parameters in the phase-field models are chosen to scale with the nondimensional interface thickness so that in the limit of vanishing interface-thickness, the sharp-interface model is recovered. Comparison of the results from the two models shows the following trends as the interface between the melt and solid is made thicker. (1) Perturbations to the plane front are stabilized as if the surface energy of the interface was increased. (2) The planar front and its perturbations behave as if the interfacial attachment kinetics was made faster, as long as the interface is significantly smaller than the capillary length. If the interface thickness is on the order of the capillary length, then the attachment kinetics may appear either slower or faster than for sharp-interface models. Stability results under "heat trapping" conditions are computed and only planar fronts whose speed increases with undercooling are found to be stable.

1

1. Introduction

The growth of a single-component crystal into its supercooled melt is often an unstable process that leads to complex morphologies of the crystal-melt interface. Using sharp-interface (or Stefan-type) models of solidification involves treating the crystal-melt interface as a zero-thickness free boundary which must be found as part of the solution. This free boundary may become quite complex geometrically, and numerical calculations that are based on explicit front-tracking of the interface position can be complicated. An alternative is to use a phase-field model for solidification (see, for example, [1]). Phase-field models approximate the crystal-melt interface as a smooth transition of finite width in the phase-field variable $\phi(x, t)$; the transition is from one value of ϕ representing the melt phase to another representing the solid phase. The constant values assumed by the phase field far from the interface each correspond to local minima in ϕ of the bulk free energy. In this type of model a nonlinear reaction-diffusion equation for the phase field is combined with the corresponding equations for the other field variables, and the resulting coupled equations are solved over the entire domain consisting of both solid and liquid phases. The regions of transition from one bulk value of ϕ to the other are identified as the crystal-melt interface, and no free boundaries must be found explicitly. The fact that phase-field models may recover sharp (zero-thickness) interface models of solidification in the limit of vanishing interface thickness has been demonstrated by Caginalp [2].

Many investigations have been carried out to compare the two modeling approaches. The critical nucleation radius for solidification and propagation of a planar front into an undercooled melt have been investigated by Caginalp and Socolovsky [3]; they find that in one-dimensional models, the interface may be a fairly large fraction of the domain size (say 20%) and still retain up to three-digit agreement with sharp-interface model results. The critical nucleation radius has also been examined by Brattkus et al. [4] with the model used by Kobayashi [5] from the perspective of a nonlinear boundary value problem. They found it necessary for the interface thickness to be smaller than the critical nucleation radius in order to get good agreement with sharp-interface predictions. The growth of a sphere modeled with each approach was also considered by Wheeler et al. [6]; their good agreement for the sphere served as justification for proceeding to computation of dendrites. A linear stability analysis of a planar front growing into a hypercooled melt has recently been carried out by Kupferman et al. [7]. In all of these cases, it is found that reasonable agreement between the two methods can be obtained provided the interface thickness is taken small enough.

Recent computations using phase-field models to compute dendritic morphologies also show the promise of this approach. Kobayashi [5] used a phase-field model to compute cellular and dendritic crystal-melt interface shapes in two dimensions, and dendritic shapes in three dimensions. Wheeler et al. [6] used a different phase-field model derived from irreversible thermodynamics [8, 9] to model two-dimensional dendritic growth. They made careful comparisons with sharp-interface theories for the Ivantsov solution, with marginal stability theory, and with microscopic solvability theory; the degree of agreement depends on the chosen parameter values. For example, the phase-field results appear to approach

marginal stability theory for smaller undercoolings; the agreement with microscopic solvability theory is better for smaller values of anisotropy. The comparison is clearly carried out in the context of a difficult problem, in which even the sharp-interface results currently constitute an area of active research.

In order to make meaningful comparisons between phase-field and sharp-interface models, it is necessary to note explicitly which parameters are being held fixed and which are allowed to vary while making the comparison. Among the parameters that appear in the phase-field model are several that have no immediate counterpart in a sharp interface model. In particular, an isotropic phase-field model generally involves a gradient energy coefficient, $(\epsilon')^2$, a double-well barrier height, $1/a'$, and a mobility parameter, M', related to the temporal relaxation of the phase field. By appealing to particular exact solutions to the phase-field equations that represent one-dimensional stationary or constant-velocity traveling wave solutions, it is possible to relate certain combinations of these phase-field parameters to more traditional parameters such as the surface energy, γ [10], and the linear kinetic coefficient, μ [11], that are often used in sharp interface treatments, together with a measure of the thickness, δ, of the diffuse interface. In this framework [12], the dependence of the exact solutions on interface thickness is such that the defining relations between the phase-field and sharp-interface parameters are valid for any value of the diffuse interface thickness. With this choice, it is also possible to show formally that in more general situations (e.g., non-planar geometries with unsteady dynamics), a sharp-interface model may be recovered from the phase-field model in the limit that the interface thickness δ is much smaller than the geometrical length scales in the problem, for fixed values of γ and μ [2]. However, in these more general circumstances, the predictions of the phase-field model and the sharp-interface model will generally disagree to some extent for values of δ that fall outside the range of asymptotic agreement of the models, despite the fact that the phase-field parameters are being constrained in an attempt to maintain common values of γ and μ. It is suggestive to compare the trends observed in the phase-field model as the interface thickness is varied with trends that are observed in the sharp-interface model when γ or μ are varied.

In this paper, we examine two cases in which the sharp-interface theory can be worked out in explicit detail, in order to obtain quantitative comparisons between sharp interface theory and phase-field theory. In the first situation, a planar front separates a crystal from its melt at the melting temperature, T_M. The front is then perturbed with a small-amplitude sinusoidal shape (following Mullins and Sekerka [13]), and the linear stability of the front examined in the context of both sharp-interface and phase-field models of solidification. In the second situation, the melt is hypercooled; that is, the bulk temperature of the melt is cooled more than L/c below the melting point, where L is the latent heat released upon solidification per unit volume and c is the specific heat of the melt at constant pressure. Under these conditions, the planar crystal-melt interface may then propagate with constant speed. The linear stability of the interface is also examined in the context of sharp and diffuse interface models. In making the comparisons, appropriate combinations of the parameters that appear in the phase-field models are held fixed, resulting in given values of the usual variables appearing in sharp-interface treatments. The diffuse-interface width can then be

varied systematically for fixed values of the sharp-interface parameters.

Important issues that arise in phase-field modeling are how small the interface thickness must be relative to the geometric length scales that occur in the problem, and also how well the time-dependent dynamical aspects of the problem are described. Both concerns are well-illustrated by dendritic growth phenomena, where the generation of secondary and tertiary sidearms produce a wide range of length scales, and the dynamical features include periodic emission of sidearms near the dendrite tip, and coarsening of the geometrical length scales farther down the primary stem on longer time scales.

In the present study using linear stability theory, we consider the dispersion relations for the sharp-interface model and phase-field models, which provide a direct quantitative dynamical comparison of the temporal growth rates for perturbations to the system. The issue of the resolution of geometrical length scales by a diffuse interface arises in the large-wavenumber limit of the dispersion relations for the phase-field models, when the wavelength of the perturbations becomes comparable to the interface thickness. One can also consider how thin an interface must be to accurately compute growth rates for long wavelength perturbations; for example, is it necessary to resolve the capillary length, even if it is much shorter than the perturbation wavelength? In addition, for the case of growth into a hyper-cooled melt, the thermal field exhibits a characteristic boundary-layer thickness κ/V, where κ is the liquid thermal diffusivity and V is the interface velocity. For a given diffuse-interface thickness, at very high growth rates this length scale becomes comparable to the interface width, and the issue of resolution can again be addressed.

A number of variations of phase-field formulations are possible, differing in detail but apparently leading to qualitatively similar results in general. We consider two formulations here: one, which was developed by Langer [1] and studied extensively by Caginalp [2], which is based on a relatively simple free energy functional, and another more recent model which is derived from a more involved thermodynamic basis [9]. Both models have similar sharp-interface limits, and have been used successfully in numerical computations.

2. Isothermal case

In this section we consider a stationary system under conditions that allow an isothermal base state, in which the solid and liquid phases are separated by a planar crystal-melt interface; the temperature of the system is the bulk melting point T_M. Since we compute the linear stability of a one-dimensional system representing a planar crystal-melt interface, our approach differs from previous work in which the spectrum was computed for isothermal perturbations to an isothermal kink [14], and for perturbations to a *uniform* phase field [15]. For ease of presentation we discuss two-dimensional perturbations to the system, with the understanding that, since the system is isotropic, linear stability results carry over to the three-dimensional case if the wavenumber is interpreted as the modulus of the three-dimensional wavevector.

2.1 Sharp interface

We first recall the linear stability results for a sharp crystal-melt interface in an isothermal system, including the effects of capillarity and interface kinetics. The interface is assumed to have the form $z' = h'(x', t')$, where z' is the coordinate normal to the mean position of the interface, x' is the coordinate along the mean position of the interface, and t' is time; the unperturbed planar interface is located at $z' = 0$. The solid occupies the region $z' < h'$ and the liquid is in $z' > h'$. We assume equal thermophysical properties in the melt and solid.

We consider the simple unperturbed solution to the problem with uniform temperature $T' = T_M$ and the stationary flat interface $h' = 0$; we examine the linear stability of this state. For the stability problem, it is convenient to nondimensionalize length with $d_0 = cT_M\Gamma/L$, which is a scaled capillary length, and time with d_0^2/κ; here κ is the thermal diffusivity, $\Gamma = \gamma/L$ is the capillary length and γ is the surface free energy of the interface. Temperature relative to the melting point is measured in units of L/c.

After nondimensionalization, the linearized perturbation equations in the bulk are

$$\frac{\partial T_L}{\partial t} = \nabla^2 T_L, \ z > 0 \text{ and } \frac{\partial T_S}{\partial t} = \nabla^2 T_S, \ z < 0; \tag{2.1}$$

at the interface we have

$$-\frac{1}{\mu}\frac{\partial h}{\partial t} = T_L - \frac{\partial^2 h}{\partial x^2}, \tag{2.2}$$

$$\frac{\partial T_L}{\partial z} - \frac{\partial T_S}{\partial z} = -\frac{\partial h}{\partial t}, \tag{2.3}$$

$$T_L = T_S, \tag{2.4}$$

where

$$\mu = \frac{\mu' T_M \Gamma}{\kappa}. \tag{2.5}$$

Here μ' is the attachment kinetics parameter; we may think of μ as a ratio of characteristic kinetic and thermal speeds. The perturbation temperatures are required to decay to zero far from the interface.

For nickel, the dimensionless kinetic coefficient is roughly $\mu = 0.05$ and the representative value of the length scale is $d_0 = 7(10^{-8})$ cm. For many situations in solidification, however, the effects of attachment kinetics are found to be insignificant and are neglected by letting μ' tend to infinity, so larger values of the parameter μ are of interest as well.

The solutions in the bulk are given by

$$T_L = T_0 \exp[\sigma t + ikx - \lambda z], \ T_S = T_0 \exp[\sigma t + ikx + \lambda z], \tag{2.6}$$

and the interface is given by

$$h = H \exp[\sigma t + ikx]. \tag{2.7}$$

Here $\lambda = \sqrt{\sigma + k^2}$, and the branch of the complex square root is assumed chosen so that the real part of λ is positive. Substitution into the interfacial conditions results in the dispersion relation

$$\sigma + \frac{\mu\sigma}{2\lambda} + \mu k^2 = 0. \tag{2.8}$$

5

By using the relation $\sigma = \lambda^2 - k^2$, this equation may be converted to a polynomial in $\lambda = \lambda(\sigma, k)$:

$$f(\lambda) = \lambda^3 + \frac{\mu}{2}\lambda^2 + k^2(\mu - 1)\lambda - \frac{\mu}{2}k^2 = 0. \tag{2.9}$$

The condition that the real part of λ should be positive usually rules out two of the three roots, leading to a single value for σ. It is easy to solve this equation numerically for the growth rate $\sigma = \sigma(k)$; this is the discrete spectrum, representing the mode which is responsible for interface instability in more general situations. There exist other solutions to the bulk equations with negative growth rates of the form

$$\sigma(k) = -k^2 - \rho^2 \tag{2.10}$$

for any positive value of ρ; the corresponding temperature fields have the form

$$T_L = T_0 \exp[\sigma t + ikx + i\rho z] + T_1 \exp[\sigma t - ikx - i\rho z], \tag{2.11}$$

and

$$T_S = T_2 \exp[\sigma t + ikx + i\rho z] + T_3 \exp[\sigma t - ikx - i\rho z], \tag{2.12}$$

and the interface shape is

$$h = H_0 \exp[\sigma t + ikx], \tag{2.13}$$

where

$$H_0 = \frac{-(T_0 + T_1)}{(k^2 + \sigma/\mu)}, \qquad T_2 = T_0 + \frac{\sigma H_0}{2i\rho}, \qquad T_3 = T_1 - \frac{\sigma H_0}{2i\rho}. \tag{2.14}$$

These solutions make up the continuous spectrum, and represent stable modes. They do not decay in the far-field; however, the analog to modes of this type may be observed in numerical calculations performed in a truncated domain. Combinations of these modes, formed by taking T_0 and T_1 to be suitable functions of ρ and integrating over ρ, do exhibit decay in the far-field.

The growth rate of the discrete mode given by Eq. (2.8) is always negative except for $\sigma(0) = 0$. Figure 1 displays results for several values of the attachment kinetics parameter μ. Asymptotic expressions for σ in the limit $k \gg 1$ can easily be obtained. We find that for $\mu < 1$,

$$\sigma = -\mu k^2 + \frac{\mu^2}{2\sqrt{1-\mu}}k + O(1). \tag{2.15}$$

For $\mu > 1$,

$$\sigma = -k^2 + \frac{\mu^2}{4(\mu - 1)^2} + O(k^{-1}). \tag{2.16}$$

For $\mu = 1$,

$$\sigma = -k^2 + \frac{1}{2^{2/3}}k^{4/3} + O(k). \tag{2.17}$$

Eq. (2.16) implies that the growth rate becomes independent of the kinetics parameter μ to leading order for $\mu > 1$; this will be useful for interpreting the differences in behavior between sharp-interface and phase-field models. For $k \ll 1$ we find that $\sigma \sim -2k^3$.

6

2.2 Phase-Field Model

Langer's phase-field model [1, 2] may be stated in nondimensional form as

$$\frac{1}{M}\frac{\partial \phi}{\partial t} = \epsilon^2 \nabla^2 \phi + \frac{1}{2}\phi(1 - \phi^2) + au, \tag{2.18}$$

$$\frac{\partial u}{\partial t} + \frac{1}{2}\frac{\partial \phi}{\partial t} = \nabla^2 u, \tag{2.19}$$

where

$$M = \frac{d_0^2 M'}{a'\kappa}, \qquad a = \frac{a'L^2}{2cT_M}, \qquad \epsilon = \frac{\epsilon'\sqrt{a'}}{d_0}, \tag{2.20}$$

subject to $u = 0$ and $\phi = \pm 1$ as $z \to \pm\infty$. We have once again nondimensionalized lengths with d_0, time with d_0^2/κ, and the temperature as $u = (T' - T_M)/(L/c)$. Here $(\epsilon')^2$ is the gradient energy coefficient, M' is a relaxation parameter, and a' is a parameter related to the barrier height in the double-well potential. In the sharp-interface limit, the parameters $(\epsilon')^2$, M', and a' may be related to the diffuse-interface thickness, the interfacial surface tension, and the interface kinetic coefficient [2]. In this model the phase-field variable ϕ varies over the range $-1 < \phi < 1$, with $\phi = -1$ representing the solid phase and $\phi = 1$ representing the liquid phase.

The dimensionless parameter ϵ represents the ratio of the diffuse interface thickness to the scaled capillary length d_0. While in order to recover the sharp-interface problem it is natural to examine the limit $\epsilon \to 0$, it should also be noted that the capillary length itself is of atomic scale, and this limit is more of a mathematical abstraction than a physically-based approximation. In this sense the limit $\epsilon \to 0$ therefore differs in some respects from the sharp interface limits used in other situations, in which the diffuse-interface thickness is taken to be small compared to macroscopic length scales in the problem, such as a container size or the radius of curvature of a nonplanar interface. The sharp-interface problem for a planar geometry in an infinite domain admits no such geometrical length scale.

Performing the asymptotic analysis in the fashion described by Caginalp [2], we find that to recover the sharp-interface model from the phase-field problem the appropriate scaling for the phase-field parameters is to take $a = \epsilon/3$, and $M = \mu/\epsilon^2$. We now choose these expressions for M and a in Eq. (2.18) for all values of ϵ, which allows us to vary the interface thickness while holding fixed the other physical parameters corresponding to the sharp-interface model. We shall return to this point in later sections.

A simple one-dimensional solution to the isothermal problem exists; it is given by

$$\bar{u}(z) = 0 \quad \text{and} \quad \bar{\phi}(z) = \tanh\left(\frac{z}{2\epsilon}\right). \tag{2.21}$$

Here we have chosen the solution which vanishes at the origin $z = 0$, where for small ϵ there is a rapid transition from solid to liquid.

We may perturb this base state as follows

$$u = 0 + \hat{u}(z)\exp[ikx + \sigma t], \qquad \phi = \bar{\phi}(z) + \hat{\phi}(z)\exp[ikx + \sigma t]; \tag{2.22}$$

7

the linearized equations for the perturbations are given by

$$\epsilon^2(D^2 - k^2)\hat{\phi} + \frac{1}{3}\epsilon\hat{u} + \frac{1}{2}(1 - 3\bar{\phi}^2)\hat{\phi} - \frac{\epsilon^2}{\mu}\sigma\hat{\phi} = 0, \tag{2.23}$$

$$(D^2 - k^2)\hat{u} - \sigma(\hat{u} + \frac{1}{2}\hat{\phi}) = 0, \tag{2.24}$$

with the far field boundary conditions

$$\hat{\phi}, \hat{u} \to 0, \qquad z \to \pm\infty. \tag{2.25}$$

We seek the growth rate $\sigma = \sigma(k, \mu, \epsilon)$ as an eigenvalue for these equations.

2.2.1   Numerical Solutions

The linearized problem given by Eqs. (2.23)-(2.25) is on an infinite domain and has variable coefficients that change rapidly in space when $\epsilon \ll 1$. The above problem is symmetric about the origin and so we need only solve the problem on the interval $0 \le z < \infty$. By testing a number of numerical schemes for treating the far-field boundary conditions, we determined that an accurate approach was to truncate the domain at a sufficiently large distance, rather than employing a coordinate transformation that maps the infinite interval to a finite interval. At the far-field boundary, the phase field is set to zero, and decay conditions are given for the thermal field. This choice is motivated by the expectation that the significant variation of the phase field is confined to an $O(\epsilon)$ vicinity of the interface, whereas outside of this region the asymptotic form of the perturbed thermal field is similar to that for the sharp interface problem. We have solved the resulting problem using two approaches. The first is to solve a boundary value problem using the FORTRAN subroutine SUPORT [16]; the growth rate σ is treated as a parameter that is varied in order to satisfy the boundary conditions in the manner described by Keller [17]. In this method, the far-field boundary condition for the perturbation temperature in the melt is replaced by $D\hat{u} = 1$ and then σ is iterated until the correct boundary condition is satisfied. The second approach is to use a pseudospectral discretization in space, followed by a numerical solution of the full matrix eigenvalue problem (See Appendix A). This procedure determines many eigenmodes for the discrete problem, and the eigenvalue with largest real part gives the growth rate corresponding to the most dangerous mode. Note that this second approach is effective in this problem because the symmetry about the origin allows us to split the domain and turn the transition in the phase field into a boundary layer. If the domain is not split in this manner, the accuracy of the pseudospectral approach is degraded due to the rapid changes in the solution in the interior of the domain [18].

Some results of the numerical solution of the problem for $\mu = 1$ and different values of ϵ are displayed in Figure 2, where the curve for $\epsilon = 0$ gives the corresponding sharp-interface results. The value $\mu = 1$ is large enough that the results correspond to the large-μ regime and are insensitive to further increases in μ. The growth rates are all nonpositive; the growth rates from the phase-field model, however, lie below those of the sharp-interface model in

general. For a given wavenumber in the indicated range, the magnitude of σ increases with ϵ, and the system becomes more stable. This effect is analogous to the effect of increasing the value of μ in the sharp-interface model (cf. Figure 1). Since μ is proportional to γ and μ', in this sense increasing the interface thickness is analogous to either an effective increase in the surface tension, as suggested by the results of Brattkus et al. [4], or to effectively faster attachment kinetics, over this range of wavenumber. Note that the interface thickness is smaller than the wavelength of the perturbation if $\epsilon k \leq 2\pi$, which is true for the indicated range of wavenumbers. For a given value of ϵ, the deviation from the corresponding sharp-interface results increases with wavenumber over the indicated range. The results of the phase-field model for a given value of ϵ might be expected to deviate significantly when the wavelength becomes comparable to the interface thickness; this will be discussed in more detail in Section 2.2.3 below.

2.2.2 Asymptotic behavior for $\epsilon \ll 1$

It is possible to apply the method of matched asymptotic expansions to the linearized problem given by Eqs. (2.23)-(2.25) to compute the correction to the sharp-interface growth rate that results from the phase-field model in the limit where the thickness of the front vanishes for a given value of k. The result of the asymptotic analysis is of the form

$$\sigma(k, \epsilon) \sim \sigma_0(k)[1 + \epsilon \sigma_1'(k)], \tag{2.26}$$

where

$$\sigma_1'(k) = \frac{2 + \sigma_0(k)/(12\lambda_0^3)}{2/\mu + 1/\lambda_0 - \sigma_0(k)/(2\lambda_0^3)}, \tag{2.27}$$

$$\lambda_0 = \sqrt{\sigma_0 + k^2}, \tag{2.28}$$

and $\sigma_0(k)$ satisfies the sharp interface dispersion relation given in Eq. (2.8).

This asymptotic behavior of the growth rate is verified in , where we compare the numerically-determined values of σ with the asymptotic results by plotting the quantity

$$s = \frac{\sigma - \sigma_0}{\epsilon \sigma_0 \sigma_1'} \tag{2.29}$$

as a function of ϵ for various wavenumbers. As expected, s converges to unity as ϵ tends to zero; the agreement is best for smaller wavenumbers, and the value of ϵ required to achieve a given accuracy decreases rapidly as the wavenumber is increased.

The quantity $\epsilon \sigma_1'$ gives the size of the relative error $(\sigma - \sigma_0)/\sigma_0$ to leading order in ϵ; the value of σ_1' is shown in Figure 4. The dependence of σ_1' on wavenumber varies considerably with μ, and for large values of μ the sign of the correction reverses for the wavenumbers $k > 1.5$. The correction to the growth rate tends to different constants depending on the value of μ. This implies that for large k, there is a small constant shift in the growth rate obtained from the sharp-interface model. Though the result stays close to the sharp interface growth rate, the asymptotic representation of the solution breaks down because the solution

to the linearized phase-field equations changes to a different behavior in the large k regime. We consider $k \gg 1$ in the next section.

Figure 3 shows that $\sigma_1' \to 0$ for $k \ll 1$; larger values of ϵ are allowed to obtain a given accuracy. Expanding Eq. (2.27) for small k shows that $\sigma_1' \sim 11k/6$, so that the relative error is small if ϵk is small; that is, if the interface width is small compared to the perturbation wavelength. This is confirmed directly from numerical calculations; for example, for $\mu = 1$, $k = 0.01$, and $\epsilon = 10$, the relative error is 18.2%, while the asymptotic result predicts 18.3%.

2.2.3 Asymptotic behavior for $k \gg 1$

When the wavelength of the perturbation to the front becomes of the order of the interface thickness or smaller, we no longer expect the phase-field model to give much physical information, but we wish to investigate how the behavior of the solutions changes in this regime. We now let ϵ be fixed, and $k \to \infty$, and examine the solutions to the linearized perturbation equations in this limit. We pose the expansions for μ bounded less than unity

$$\sigma = \Sigma_0 k^2 + \Sigma_2 + \ldots, \tag{2.30}$$

$$\Phi = \Phi_0(z) + \frac{1}{k^2}\Phi_2(z) + \ldots, \tag{2.31}$$

$$U = U_0(z) + \frac{1}{k^2}U_2(z) + \ldots . \tag{2.32}$$

Substitution into the linearized equations Eqs. (2.23)-(2.25) yields to leading order that

$$U_0 = \frac{-\Sigma_0}{2(1 + \Sigma_0)}\Phi_0, \text{ and } \Sigma_0 = -\mu. \tag{2.33}$$

At next order, we find that

$$\epsilon^2 D^2 \Phi_0 - Q(z)\Phi_0 = 0, \tag{2.34}$$

where

$$Q(z) = -\frac{1}{2}[1 - 3\bar{\phi}^2(z)] + \frac{\epsilon\Sigma_0}{6(1 + \Sigma_0)} + \frac{\epsilon^2\Sigma_2}{\mu} \tag{2.35}$$

This is an eigenvalue problem for Σ_2; the problem has some analogy with the motion of a particle in a potential well given by the first two terms of $Q(z)$ and an energy given by the last term in Q. A solution of the form

$$\Phi_0 = \text{sech}^2\left(\frac{z}{2\epsilon}\right), \tag{2.36}$$

$$\Sigma_2 = \frac{\mu^2}{6\epsilon(1 - \mu)} \tag{2.37}$$

may be found; further terms in the series may also be constructed by continuing the procedure.

Numerical solution of Eq. (2.34) shows that this is the first eigenfunction and eigenvalue; higher modes have sign changes near the origin and do not exhibit decay for large $|z|$. We

10

believe these modes to be analogs to the continuous spectrum of the sharp interface model on an infinite domain. In the limit $\epsilon \to 0$, the expansion for $k \gg 1$ breaks down. Compare the expansion in this limit with the sharp-interface expansion for $k \gg 1$ and $\mu < 1$, Eq. (2.15). It is now clear how the two limits $\epsilon \to 0$, k fixed and $k \gg 1$, ϵ fixed do not interchange.

A similar approach may be employed for μ bounded above unity. We make a change of variable $z = k\hat{z}$, so that $D^2 \to \hat{D}^2/k^2$ where $\hat{D} = d/d\hat{z}$; we pose the expansions

$$\sigma = \Sigma_0 k^2 + \Sigma_2 + \dots, \tag{2.38}$$

$$\Phi = \frac{1}{k^2}(\Phi_0(\hat{z}) + \frac{1}{k^2}\Phi_2(\hat{z}) + \dots), \tag{2.39}$$

$$U = U_0(\hat{z}) + \frac{1}{k^2}U_2(\hat{z}) + \dots . \tag{2.40}$$

At leading order, we find that $\Sigma_0 = -1$, and that

$$U_0 = \frac{3\epsilon(\mu - 1)}{\mu}\Phi_0. \tag{2.41}$$

At $O(1)$, we find that

$$\Sigma_2 = \frac{\mu}{6\epsilon(\mu - 1)}; \tag{2.42}$$

a bit of algebra at $O(k^2)$ yields the equation

$$\left\{ \frac{3\epsilon(\mu - 1)}{\mu}\hat{D}^2 + \frac{\mu}{2\epsilon^2(\mu - 1)} \left[\frac{1}{2}(1 - 3\bar{\phi}^2) + \frac{\epsilon^2 \Sigma_2}{\mu} \right] \right\} \Phi_0 = 0. \tag{2.43}$$

Again we find that the first two terms for the growth rate are determined by an outer problem; the leading order eigenfunctions are determined as well. Solutions to Eq. (2.43) were obtained numerically using a pseudospectral discretization in space, and again solving the resulting matrix eigenvalue problem for the function values at the collocation points. The solutions to the asymptotic problem again correspond to the first eigenvalue and eigenfunction.

2.3   Discussion

A summary of the numerical and asymptotic results is presented in Figures 5 and 6. In these figures the numerical results are compared to the asymptotic results; we find that for smaller wavenumbers, the asymptotics for $\epsilon \ll 1$, $k = O(1)$ are a reasonable approximation to the numerically computed results, while for larger values of k, the asymptotic results in the limit $k \gg 1$, $\epsilon = O(1)$ are a good approximation. The numerical results illustrate the transition between the types of behavior. The "rolling off" of the diffuse interface results for larger k is an indication that the interface no longer resolves the short-wavelength perturbations, and is now qualitatively different than the sharp-interface model. Qualitatively similar results are obtained when the phase-field model I of Wang et al. [9] is analyzed in the same manner. We believe this departure to be generic for large wavenumber perturbations in diffuse interface models. We note that from Figure 2-4, it is apparent that long waves are much easier to resolve; this is true in the sense of being in the asymptotic regime where sharp-interface asymptotics is valid.

3. Hypercooled case

If the melt is cooled by more than L/c below the melting point, the melt is said to be hypercooled and the solid phase may grow at constant speed [19]. Sharp interface models of solidification have constant speed solutions for undercoolings larger than L/c [19]. For these large undercoolings, there is no time-dependent buildup of heat ahead of the front as it propagates and the growth of the solid phase is limited by attachment kinetics. This situation is difficult to achieve experimentally for metals (for example [20,21]), but it has been achieved for the molecular material white phosphorus (P_4) in a directional apparatus [19]. Several theories of the linear and nonlinear stability of the planar sharp interface have been developed [22–27]. Generally, the planar front is unstable to long waves; however, when the undercooling is sufficiently large, the planar front is restabilized according to linear theory. For our purposes, the theory is well understood in that the roles of the material parameters are known and can provide for a good comparison between sharp-interface and phase-field modeling approaches. The phase-field model we will employ is model I of Wang *et al.* [9].

Several investigations near supercooling of L/c have been carried out for phase-field models. Collins and Levine [28] computed plane front solutions for Langer's phase-field model. Schofield and Oxtoby [29] examined essentially the same model at exactly L/c undercooling and found that constant velocity solutions only exist for sufficiently low thermal diffusivities; Löwen *et al.* [30, 31] examined the same situation for a piecewise parabolic free energy (the "parabolic" model), and found similar behavior. Löwen and Bechhoefer [31] computed constant speed solutions for other supercoolings near L/c analytically and found that constant speed solutions could exist at smaller supercoolings than L/c. A time-dependent computational approach was used to find these constant speed solutions in [32]; Umantsev [33] has computed the same type of solution for a different phase-field model similar to that of model II in Wang *et al.* [9]. The stability of these constant-speed solutions had been examined only for planar perturbations by Umantsev [33]; our work will be more general in that we allow corrugations to the planar front. Recently a stability calculation has been carried out for a parabolic phase-field model [7]; their results will be discussed with the results of the present work.

3.1 Sharp Interface Model

We begin by summarizing sharp interface results in our notation. A pure crystal grows into a hypercooled melt; that is, the far field temperature in the melt is given by $T_\infty < T_M - L/c$. We write the governing equations in a frame moving with speed V_0 in the positive-z direction; we also replace the far-field boundary conditions with

$$T_L \to T_\infty,\ z \to \infty,\ \text{and}\ T_S \to T_\infty + L/c,\ z \to -\infty. \tag{3.1}$$

We again nondimensionalize lengths with $d_0 = T_M \Gamma c / L$ and time with d_0^2/κ, but the temperature is now scaled with $T_M - T_\infty$. After nondimensionalization, the base state (a function

of z only) becomes

$$T_{0L} = -1 + \frac{e^{-\mathcal{P}z}}{\Delta}, \qquad T_{0S} = -1 + \frac{1}{\Delta}; \tag{3.2}$$

the constant pulling speed is given by the nondimensional Pèclet number as

$$\mathcal{P} = \mu(\Delta - 1), \tag{3.3}$$

where

$$\mathcal{P} = V_0 d_0 / \kappa, \ \Delta = \frac{c(T_M - T_\infty)}{L}, \tag{3.4}$$

and μ is defined as before.

The linear disturbance equations in the bulk are just the diffusion equations with drift

$$\frac{\partial T_L}{\partial t} + \mathcal{P} \frac{\partial T_L}{\partial z} = \nabla^2 T_L, \ z > 0; \tag{3.5}$$

$$\frac{\partial T_S}{\partial t} + \mathcal{P} \frac{\partial T_S}{\partial z} = \nabla^2 T_S, \ z < 0; \tag{3.6}$$

at $z = 0$ we have

$$-\frac{1}{\mu\Delta} \frac{\partial h}{\partial t} = T_L + \frac{\partial T_{0L}}{\partial z} h - \frac{1}{\Delta} \frac{\partial^2 h}{\partial x^2}, \tag{3.7}$$

$$\Delta \left(\frac{\partial T_L}{\partial z} - \frac{\partial T_S}{\partial z} + \frac{\partial^2 T_{0L}}{\partial z^2} h \right) = -\frac{\partial h}{\partial t}, \tag{3.8}$$

$$T_L + \frac{\partial T_{0L}}{\partial z} h = T_S. \tag{3.9}$$

The perturbation temperatures must decay to zero far from the interface.

The solutions are given by

$$T_L = T_1 \exp[\sigma t + ikx + \lambda_L z], \tag{3.10}$$

$$T_S = T_2 \exp[\sigma t + ikx + \lambda_S z], \tag{3.11}$$

and

$$h = H_1 \exp[\sigma t + ikx]; \tag{3.12}$$

here

$$\lambda_L = -\frac{\mathcal{P}}{2} - \hat{\lambda}, \ \lambda_S = -\frac{\mathcal{P}}{2} + \hat{\lambda}, \ \text{and} \ \hat{\lambda} = \sqrt{\frac{\mathcal{P}^2}{4} + \sigma + k^2}. \tag{3.13}$$

Substitution into the interfacial conditions and eliminating the explicit σ dependence results in the dispersion relation

$$\hat{\lambda}^3 + \frac{\mu}{2}\hat{\lambda}^2 + \left[(\mu - 1)k^2 - \frac{\mu\mathcal{P}}{2} - \frac{\mathcal{P}^2}{4} \right] \hat{\lambda} - \frac{\mu}{2}k^2 + \frac{\mu\mathcal{P}^2}{8} = 0. \tag{3.14}$$

13

This equation is easily seen to reduce to the isothermal case by setting $\mathcal{P} = 0$. The modes corresponding to the solution of this equation are the discrete part of the spectrum. Solutions to the bulk equations also exist with

$$\sigma = -\frac{\mathcal{P}^2}{4} - k^2 - \rho^2, \ 0 < \rho < \infty; \tag{3.15}$$

these modes are the continuous spectrum. Again these modes do not satisfy the decay boundary conditions, but they can be important in interpreting numerical results on a finite domain.

It is easy to solve this equation numerically for the growth rate $\sigma = \sigma(k)$. Long waves are found to be unstable, while short waves are stabilized by capillarity. The restabilization of the planar front at high speed, or absolute stability [22–27], is readily seen as the nondimensional speed $\mathcal{P}$ increases. As $\mathcal{P}$ increases, the band of unstable wavenumbers shrinks and for $\mathcal{P} \geq 1$, there are no wavenumbers with positive growth rate. This result has been examined by a number of authors. [22–25, 27] A simple result sufficient for our purposes is that for $k \ll 1$ and $\mathcal{P}$ a bounded amount (with respect to k) away from 0 and 1, we have

$$\sigma \sim \mu \frac{1 - \mathcal{P}}{\mathcal{P}} k^2. \tag{3.16}$$

Sharp interface results will be compared with phase-field results in the next section.

3.2   Phase-Field Model

A phase-field model of Wang *et al.* [9] (their model I) may be nondimensionalized with the length scale d_0, the time scale d_0^2/κ, and the temperature relative to T_M in units of the undercooling $T_M - T_\infty$; shifting to a reference frame moving with speed V_0 in the positive-z direction, we obtain

$$\frac{\partial \phi}{\partial t} - \mathcal{P}\frac{\partial \phi}{\partial z} = M\left[ap'(\phi)u - \frac{1}{120}p''(\phi) + \epsilon^2\nabla^2\phi\right], \tag{3.17}$$

$$\frac{\partial u}{\partial t} - \mathcal{P}\frac{\partial u}{\partial z} + \frac{1}{\Delta}p'(\phi)\left(\frac{\partial \phi}{\partial t} - \mathcal{P}\frac{\partial \phi}{\partial z}\right) = \nabla^2 u, \tag{3.18}$$

where

$$M = \frac{d_0^2 M'}{a''\kappa}, \ a = \frac{a''L(T_M - T_\infty)}{T_M^2}, \ \epsilon = \frac{\epsilon''\sqrt{a''}}{d_0}, \tag{3.19}$$

and

$$p(\phi) = \phi^3(10 - 15\phi + 6\phi^2). \tag{3.20}$$

Here $(\epsilon'')^2$ is a gradient entropy coefficient and $1/a''$ is related to the barrier height (see [9] for more detail). We require that $u = -1$, $\phi = 1$ as $z \to \infty$ and $u = u_S$, $\phi = 0$ as $z \to -\infty$; here u_S is a constant to be determined.

14

As done previously, we may take the limit $\epsilon \to 0$ to recover the sharp-interface model. After an analysis similar to that done by Caginalp [2] (all details are omitted), the appropriate scales are $a = \alpha\epsilon\Delta$, $M = \mu/\epsilon^2$, $\Delta = O(1)$ where $\alpha = 1/(6\sqrt{2})$. We now choose the parameters in the phase-field model to follow this scaling, regardless of the size of ϵ; that is we fix μ and Δ, while ϵ varies.

The phase-field parameters may be related to the physical parameters of the sharp-interface models in the following way. We choose the physical interface thickness δ to be

$$\delta = \epsilon''\sqrt{a''}. \tag{3.21}$$

Redimensionalizing results in the following expressions for the phase-field parameters in terms of the sharp-interface model parameters:

$$\epsilon'' = \sqrt{\frac{\gamma\delta}{\alpha T_M}}, \quad a'' = \frac{\alpha T_M}{\gamma}\delta, \text{ and } M' = \frac{\mu' T_M^2 \alpha}{L}\frac{1}{\delta}. \tag{3.22}$$

From these relations, it is clear that varying only ϵ in the nondimensional parameters is equivalent to varying the physical interface thickness δ while holding the other physical parameters fixed.

3.2.1 The plane front

We may look for one-dimensional solutions to the hypercooled problem. We must solve the time-independent, one-dimensional form of Eq. (3.17) and Eq. (3.18) subject to the boundary conditions

$$\phi \to 0, \, u \to u_S \text{ as } z \to -\infty \text{ and } \phi \to 1, \, u \to -1 \text{ as } z \to \infty. \tag{3.23}$$

The solution must be calculated numerically in general. It is convenient to integrate the thermal equation once (from z to ∞) to obtain

$$u_z + \mathcal{P}\left[u + \frac{1}{\Delta}p(\phi)\right] = \mathcal{P}(\frac{1}{\Delta} - 1). \tag{3.24}$$

From this first integral, it is clear that as $z \to -\infty$ that the solid temperature becomes identical to the sharp-interface model, i.e. $u_S = -1 + 1/\Delta$ [19], even when the interface has a finite width.

For the purposes of numerical approximation, we truncate the domain. We may minimize the error involved by applying boundary conditions on the phase field that enforce the same decay as would occur in the infinite domain. This is accomplished by linearizing around the phase field values of zero and unity to find the decay to these states, and imposing boundary conditions to enforce this decay. The result for the solid far from the interface ($z = -z_l$) is

$$\phi_z - \lambda_+\phi = 0; \tag{3.25}$$

in the melt far from the interface ($z = z_l$), we have

$$\phi_z - \lambda_-(\phi - 1) = 0, \tag{3.26}$$

15

where

$$\lambda_\pm = -\frac{\mathcal{P}}{2\mu} \pm \sqrt{\left(\frac{\mathcal{P}}{2\mu}\right)^2 + \frac{1}{2\epsilon^2}}. \tag{3.27}$$

The different decay rates are a consequence of the asymmetry in the hypercooled case. The above boundary value problem involving the second order equation for the phase field, the first order temperature equation, the asymptotic boundary conditions on the ends of the domain $|z| < z_L$ and the single temperature boundary condition of $u(-z_L) = -1 + 1/\Delta$ is solved using the package COLNEW [34]. We have also used the appropriate Dirichlet conditions at the boundaries. We can easily converge to results independent of the boundary conditions and the domain length when ϵ and Δ are not too large.

This boundary value problem is a nonlinear eigenvalue problem (for the heteroclinic orbit in phase space that connects the fixed points $(\phi, \phi_z, u) = (0, 0, -1 + 1/\Delta)$ and $(\phi, \phi_z, u) = (1, 0, -1)$; similar solutions to a different phase-field model have been given by Umantsev [33] in his Figure 2. We seek the eigenvalue $\mathcal{P} = \mathcal{P}(\epsilon, \mu, \Delta)$. In order to find the nondimensional speed $\mathcal{P}$ we fix the value of the phase field at the origin as $\phi(0) = 1/2$ and solve the boundary value problems arising for positive and negative z separately. In general, the slope of the phase field at the origin will not be continuous, and we use the difference of the slopes as a residual for iterating on $\mathcal{P}$. Both DNSQ [35] and DFZERO [36, 37] have been used for root finders in the iteration. A representative solution is shown in Figures 7 and 8; in these figures, the characteristic length of the thermal field is larger than the layer thickness in the phase field. For a fixed ϵ, we find that for smaller Pèclet numbers the decay length of the thermal field is much longer than the layer thickness and for large Pèclet numbers the two fields have the same characteristic length. This behavior has been pointed out by Umantsev [33].

Figures 9-11 display results for the propagation of the plane front into the melt. The constant speed solutions indicated by the curves deviate from the sharp-interface results as ϵ increases. Constant speed solutions are found for undercoolings smaller than unity when the interface attachment kinetics parameter μ and nondimensional interface thickness ϵ are large enough; we have chosen a very large value of the kinetics parameter $\mu = 10$ in Figure 9 for ease of demonstration. Such solutions have been found by previous workers [31–33]; we shall come back to a comparison with their findings. For smaller values of the kinetics parameter μ the constant speed solutions deviate much less from the sharp-interface results for comparable interface thicknesses; Figure 11 displays the magnified deviations from the sharp interface results for $\mu = 0.05$. No sub-unit-undercooling constant-speed solutions exist.

Constant-speed solutions below unit undercooling do occur, as shown in Figure 9, when the quantity $\mu\epsilon$ increases through (approximately) unity; this was empirically determined for $5 < \mu < 20$. Specifically, numerical calculations show that

$$\mu\epsilon = \frac{\mu'L}{c} \cdot \frac{\epsilon'\sqrt{a'}}{\kappa} \approx 1.5 \tag{3.28}$$

The product $\mu\epsilon$ thus gives a ratio of kinetic to thermal speeds. When the thermal diffusion speed becomes smaller than the kinetic speed, constant speed solutions for $\Delta < 1$ may occur.

16

This behavior is in qualitative agreement with the results of previous work [29–32]. We note, however, that our work differs from theirs in the treatment of the nondimensional parameter a; in their work, the equivalent parameter does not vary with ϵ.

We also note that when the front propagates at constant speed for an undercooling less than unity, the solid formed is superheated [31,32]. Superheated solid was not observed with the growth of white phosphorus (P_4) into its hypercooled melt [19] For P_4,we estimate $\mu = 0.066$ based on [19,38] and references therein; thus our model would not predict superheated solid. Löwen $et\ al.$ [31,32] have discussed the possibility of this behavior for solution growth.

3.2.2 Linear Theory

We perturb the transition layer as follows:

$$\phi = \bar{\phi}(z) + \Phi(z)e^{ikx+\sigma t}, \quad \text{and} \quad u = \bar{u}(z) + U(z)e^{ikx+\sigma t}. \tag{3.29}$$

The linearized perturbation equations are

$$\epsilon^2(D^2 - k^2)\Phi - \frac{p'''(\bar{\phi})}{120}\Phi + \alpha\Delta\epsilon\left[p''(\bar{\phi})\bar{u}\Phi + p'(\bar{\phi})U\right] - \frac{\epsilon^2}{\mu}\left[\sigma\Phi - \mathcal{P}D\Phi\right] = 0, \tag{3.30}$$

$$(D^2 - k^2)U - \sigma U + \mathcal{P}DU - \frac{1}{\Delta}\left[p'(\bar{\phi})\sigma\Phi - \mathcal{P}p''(\bar{\phi})\bar{\phi}_z\Phi - \mathcal{P}p'(\bar{\phi})D\Phi\right] = 0, \tag{3.31}$$

subject to $\Phi, U \to 0$ as $|z_l| \to \infty$; here $D = d/dz$.

Based on experience with the isothermal model, we truncate the domain rather than map. The truncation of the domain is a little more complicated than for the isothermal model; the approach here is to linearize around the states $\phi = 0, 1$ and impose the boundary conditions at $\pm z_l$ such that the appropriate decay is recovered. These boundary conditions are, on $z = z_l$,

$$\Phi_z - \lambda_-^{(\Phi)}\Phi = 0, \quad \text{and} \quad U_z - \lambda_-^{(T)}U = 0; \tag{3.32}$$

on $z = -z_l$, we have

$$\Phi_z - \lambda_+^{(\Phi)}\Phi = 0, \quad \text{and} \quad U_z - \lambda_+^{(T)}U = 0. \tag{3.33}$$

Here

$$\lambda_\pm^{(\Phi)} = -\frac{\mathcal{P}}{2\mu} \pm \sqrt{\left(\frac{\mathcal{P}}{2\mu}\right)^2 + \frac{\sigma}{\mu} + k^2 + \frac{1}{2\epsilon^2}}, \tag{3.34}$$

and

$$\lambda_\pm^{(T)} = -\frac{\mathcal{P}}{2} \pm \sqrt{\left(\frac{\mathcal{P}}{2}\right)^2 + \sigma + k^2}. \tag{3.35}$$

Note that the boundary conditions for the temperatures are only approximated for ϕ near zero and one, and so the temperature need not be too close to its final value; in effect, we are only integrating through the layer in ϕ. This is expected to help with the typically slower decay of the thermal field.

3.2.3 Numerical Solution Schemes

We employ two methods of solving the problem numerically. The first is a finite difference approximation, where the maximum eigenvalue of a matrix from the discrete problem yields the growth rate of the perturbations. The second is a shooting method, where the growth rate is found as an eigenvalue in a boundary value problem; the problem is solved using the routine SUPORT. The two approaches are complementary; the finite-difference method can find the first few modes, and the results of this approach may be used as good guesses for the more accurate boundary-value-problem approach.

In the finite difference approach, we use second-order accurate central differences for first and second derivatives at the interior points. For the boundary conditions we use a forward or backward approximation. The boundary conditions pose a problem because they contain functions of the eigenvalue σ when the decay conditions are applied on the truncated domain. We can only eliminate one of the radicals at a time via substitution; we choose to retain the decay conditions on the thermal field, because the decay is typically slower for that field in the parameter range of interest. We then further approximate the linearized problem with the Dirichlet conditions for the phase $\Phi = 0$ on $z = \pm z_l$. Using the approach outlined in [39], we employ a scheme in which the size of the discrete system is roughly doubled in order to put the equations in standard generalized eigenvalue form (see Appendix B for details). Solving the algebraic generalized eigenvalue problem yields more than just the first eigenvalue and eigenmode, and this may be of value in discovering nearby modes; it may also yield good starting values for our more accurate, second approach.

In the second approach, we use Keller's method [17] as a means of iterating with σ in order to satisfy all of the boundary conditions in the problem. In this approach, we replace the decay condition in the melt with the condition $Du = 1$, and then iterate with σ until the decay condition is satisfied. This method has the advantage of high accuracy, but its convergence to the result is often very sensitive to the initial guess. The decay boundary conditions at each end of the domain present no difficulty as well. For simplicity, we apply the Dirichlet conditions $\Phi = 0$ on the boundaries as in the finite difference implementation. It is possible to compute the solution to a given error tolerance with either the decay or Dirichlet conditions on $\bar{\phi}$ in the base state, and so we believe this to be a reasonable approximation.

3.2.4 Linear Theory Results

The growth rate of the perturbations to the planar front propagating into a hypercooled melt are displayed in Figure 12. By decreasing ϵ, the growth rates can be made as close as one likes to the sharp interface results, although under extreme conditions accurate computations can be rather difficult to carry out. Long waves are again unstable and short waves are stable. The growth rates of the long waves are increased. We find this to be consistent with the interface attachment kinetics being apparently more rapid. The growth rates for the two models cross at some wavenumber for $\sigma < 0$, and the phase-field growth rates are lower (more negative) thereafter for larger k. We find this consistent with an apparently higher surface energy for the phase-field models. This is born out by the comparison of the absolute stability

limit shown in Figure 13; the absolute stability limit occurs at lower undercoolings and higher speeds than for the sharp-interface model as the thickness of the interface increases. One instance of distinguishing the different restabilizations of the interface is illustrated in Figure 14; this determination is approximate because the numerical error becomes more important in finding accurate solutions for very small wavenumbers.

We may compute the marginally stable wavenumber $k_0 > 0$ for which $\sigma = 0$; the results for two different approaches is shown in Table 1. This case was chosen based on choosing a representative growth speed of 2000 cm/s for a nickel dendrite [41] with $\mu = 0.05$. The sharp interface result is listed in the first line; in the second line we match the undercooling and in the third we match the speed. It is apparent that most of the modification of the marginal wavenumber, and most likely in the rest of the linear theory, is due to the modification of the base state. It is possible to use k_0 in marginal stability theory for the tip of a growing dendrite [40] (when the speeds are matched); based on the small error observed in the calculations, one would expect the difference in the predictions for the sharp- and diffuse-interface theories to be very similar. Note that the comparison that is made for the purposes of marginal stability theory is for fixed speed $\mathcal{P}$; alternatively, one can also compare the results with the bulk undercooling fixed. We note that in either case further increase in ϵ over the values shown in Table 1 results in a complex growth rate.

In Figure 15, we illustrate linear stability results for $\mu = 10$, $\epsilon = 0.25$; for these parameter values, constant-speed solutions exist for undercoolings less than unity. The growth rates for the first two modes are shown above, below and at the limit point; similar behavior is seen for other parameter values. We find that the part of the base state that has negative slope in the $(\Delta, \mathcal{P})$-plane is indeed unstable; the modes may be real or complex depending on the parameters.

It is interesting to note the double-zero in the growth rate at the limit point as illustrated in Figure 15, at the point labeled b. We note that the eigenfunctions for the two modes are rather similar for the parameters we have studied. The growth rate as a function of $\mathcal{P}$ for fixed $k = 0.1$, $\mu = 10$, $\epsilon = 0.25$ is shown in Figure 16; the longer the wavelength of the perturbation, the larger the value of $\mathcal{P}$ required before that mode restabilizes. All wavenumbers are stable above the limit point, save $k = 0$ which is neutrally stable. Note that in Figure 15, at the point a in the $(\mathcal{P}, \Delta)$-plane, there is a possible Hopf bifurcation for a fixed $k \approx 0.063$; if such a bifurcation occurs, there is a good possibility that it is of Takens-Bogdanov type [42]. The nonlinear analysis of the equations to substantiate this possibility are beyond the scope of this paper.

3.3 Discussion

The phase-field model we use has plane front solutions similar in some respects to other phase-field models. In particular, the convergence of the phase-field model to the sharp interface model for vanishingly thin interfaces, and the existence of constant speed solutions below unit undercooling are two of the similarities. Löwen and Bechhoefer [31] gave a physical argument suggesting that the states where $\mathcal{P}$ increases with decreasing Δ are unstable. Such

states were found to be unstable to planar perturbations by Umantsev [33] in a different model; the upper branch where the speed increases with increasing undercooling was found to be stable against planar perturbations. We have computed the stability of the plane front against sinusoidal perturbations; on the upper branch, we find neutral stability for a planar perturbation. Because of the large value of μ required to access constant speed solutions below unit undercooling, any states that appear linearly stable in the regime $\Delta < 1$ seem unlikely to occur physically for a thermal problem, as discussed in [31], and such states have not been observed in P_4 [19]. Umantsev has given this growth of the superheated solid at constant speed the name "heat trapping" [33], making an analogy with solute trapping in the rapid directional solidification of an alloy (see, for example, [43]).

The observed differences between the phase-field and sharp-interface models may be explained by analogy with sharp interface results with an increased surface energy γ and an increased attachment kinetics parameter μ', provided that the diffuse interface thickness in the phase-field model is smaller than about 10% of the capillary length d_0. This is based on a number of facts. Planar fronts calculated from Model I of Wang *et al.* [9] traveled faster than their sharp interface counterparts for $\epsilon \leq 0.1$, approximately. For thicker interfaces, fronts slower than those of the sharp-interface model for the same μ and Δ can occur (see Figures 10 and 11). For the hypercooled case, the growth rates σ of the unstable modes of the phase-field model with small wavenumber are increased over the corresponding sharp-interface wavenumbers (see Figure 12); based on the asymptotic form of the growth rate for the sharp-interface model Eq. (3.16), this seems reasonable.

For large enough wavenumbers the phase-field growth rates are lower (more stable) than the sharp-interface results, and so in this capillarity-dominated regime, it appears that the thick interface has a higher apparent surface energy. This conclusion is in agreement with recent results obtained by Brattkus *et al.* [4]. They studied the effect of thickening the interface on the critical nucleation radius of a seed in an undercooled melt; their static calculation provided a good comparison for apparent surface energy. They found that the sharp-interface model required a higher surface energy to have the same nucleation radius as a seed in the phase-field model; the phase-field model thus had a higher apparent surface energy in two dimensions. We note that in [4], it was found that for a small regime in the three-dimensional case there was an apparent reduction in the surface energy; given the isotropic nature of our work, no such trend in the linear problems we have studied. The linear theory of our work also shows that absolute stability also occurs (though modified) for the planar interface in the phase-field model; absolute stability was also observed in the parabolic model studied in [7].

The constant speed solutions of Kupferman *et al.* [7], for a model with a piecewise-parabolic potential, grow faster than a linear relationship with undercooling, yet all emanate from unit undercooling with positive slope, like the sharp-interface model (their Figure 6). Apparently, in their parabolic model, the interface attachment kinetics become faster relative to sharp interface behavior with increasing undercooling according to planar state results. Their computed growth rates also show that short waves are more stable in their phase-field model than in the sharp-interface model for the range of data they present (their Figure 7);

thus the surface energy is apparently increased for their model as well; the linear theory results for small wavenumbers show a stabilization of the long waves; this suggests that the attachment kinetics are apparently slower according to their linear theory. We see either stabilization or destabilization of long waves.

Interpretation of the apparent increase in the surface energy of the diffuse interface seems straightforward. The interface is harder to corrugate when it takes on some thickness; level curves of ϕ must be distorted and this takes some of the free energy of the system. In the limit of vanishing thickness of the interface this distortion vanishes. The behavior of the apparent attachment kinetics is more complicated; there does not seem to be any single trend as the interface thickness increases in the base state.

4. Conclusion

We have computed plane-front, constant-speed solutions to sharp and diffuse interface models for solidification of a hypercooled melt. We have undertaken an investigation of what happens quantitatively to morphological instability results when the crystal-melt interface thickness is allowed to be nonzero.

The stability of an isothermal plane front against sinusoidal perturbations was considered in order to contrast some of the behavior of phase-field and sharp-interface models. We investigate the limits $\epsilon \ll 1$, k fixed and $k \gg 1$, ϵ fixed, and showed how the two regimes compared with numerical solutions to the problem. We found an apparent increase in the product of the surface energy and attachment kinetics coefficients. The large k behavior of the diffuse-interface model deviated qualitatively from the sharp-interface model. When k is not large, the interface thickness need only be small compared to the perturbation wavelength to obtain a small error in the perturbation growth rate relative to sharp-interface theory.

The base state and linear stability results for growth of a crystal into its hypercooled melt indicated that as long as the interface was not too diffuse, then the attachment kinetics were apparently enhanced and the surface energy of the interface apparently increased by the use of phase-field models. For thicker fronts, the kinetics may be faster or slower. Based on our calculations, it appears that one must require the thickness of the front to be comparable to or smaller than the capillary length d_0 in order to get good agreement with sharp-interface theories in both the base state and the linear stability results. For small μ, an interface thickness comparable to the capillary lenght appears to give acceptable results; for a large μ, an interface thickness significantly smaller than the capillary length is required in order to mimic sharp-interface results.

Acknowledgements

Appendix A.   Pseudospectral Discretization

We discretize the derivatives in the z direction using the standard Chebyshev pseudospectral method (see, e.g., [44, 45]). It is convenient for this method to rescale z as

$$z = \frac{1}{2}(\xi + 1)z_l \tag{A.1}$$

in order to map the domain on the half interval $0 \le z \le z_l$ to $-1 \le \xi \le 1$. We then have $d/dz = (2/z_l)d/d\xi$. We take advantage of the symmetry of the linearized equations to solve the problem over the half interval so that the region of rapid change in the coefficients occurs at the boundary of the interval; this alleviates the Gibbs phenomenon which occurs if the rapid transition occurs in the interior of the domain [18]. At $z = 0$ we have $d\phi/dz = du/dz = 0$, and at $z = z_l$ we have $\phi = u = 0$.

We use the points $\xi_j = \cos j\pi/n$ for $j = 0, 1, \ldots, n$, so that the "interface" is located at $\xi_n = -1$. At the collocation points we use the Chebyshev derivative matrix D_{ij} [45], which has the property that at the collocation points ξ_j the derivative g'_j of an n-th degree polynomial $g(\xi)$ is given exactly in terms of its collocation values g_k by the expression

$$g'_j = \sum_{k=0}^{n} D_{jk}g_k. \tag{A.2}$$

Higher derivatives are represented by powers $D_{ij}^{(m)}$ of the matrix D_{ij}. We write $g'_j = D_{jk}g_k$ and thereby let the sum over the repeated index k be implied.

At the interior points in the melt ξ_j, $j = 1, \ldots, n-1$, we have the discrete equations

$$\epsilon^2 (D_{ij}^{(2)} - k^2 \delta_{ij})\phi_j - \frac{\sigma}{M}\delta_{ij}\phi_j + \frac{1}{2}(1 - 3\phi_{0i}^2)\delta_{ij}\phi_j + a\delta_{ij}u_j = 0, \tag{A.3}$$

$$(D_{ij}^{(2)} - k^2 \delta_{ij})u_j - \sigma\delta_{ij}(u_j + \frac{1}{2}\phi_j) = 0, \tag{A.4}$$

where i and j range from 1 to n. The boundary conditions become $D_{nj}\phi_j = D_{nj}u_j = 0$; note that $\phi_0 = u_0 = 0$. The discrete equations then have the form

$$\mathbf{Ax} = \sigma\mathbf{Bx}, \tag{A.5}$$

which is algebraic generalized eigenvalue problem.

Appendix B. Finite-Difference Discretization

We use central differences for the second order spatial derivatives and for the first order derivatives we use a central difference with twice the step size to discretize Eqs. (3.30), (3.31), and thermal conditions in (3.32) and (3.33). For the boundary conditions we use a forward or backward approximation with a single grid step. The boundary conditions pose a problem because they contain functions of the eigenvalue σ when the decay conditions are applied on the truncated domain. We define

$$s_T = \sqrt{\mathcal{P}^2/4 + \sigma + k^2}, \tag{B.1}$$

which allows us to rewrite the problem as

$$\epsilon^2(D^2 - k^2)\Phi - \frac{p'''(\bar{\phi})}{120}\Phi + \alpha\Delta\epsilon\left[p''(\bar{\phi})\bar{u}\Phi + p'(\bar{\phi})U\right] - \frac{\epsilon^2}{\mu}\left[(s_T^2 - \mathcal{P}^2/4 - k^2)\Phi - \mathcal{P}D\Phi\right] = 0, \tag{B.2}$$

$$D^2U - (s_T^2 - \mathcal{P}^2/4)U + \mathcal{P}DU - \frac{1}{\Delta}\left[p'(\bar{\phi})(s_T^2 - \mathcal{P}^2/4 - k^2)\Phi - \mathcal{P}p''(\bar{\phi})\bar{\phi}_z\Phi - \mathcal{P}p'(\bar{\phi})D\Phi\right] = 0, \tag{B.3}$$

subject to $\Phi = 0$ at $z = \pm z_l$, and

$$U_z - (-\mathcal{P}^2/4 - s_T)U = 0, \quad z = z_l, \tag{B.4}$$

$$U_z - (-\mathcal{P}^2/4 + s_T)U = 0, \quad z = -z_l. \tag{B.5}$$

The grid is given by $z_j = -z_l + (j-1)\Delta z$ so that $z_1 = -z_l$ and $z_n = z_l$, and $\Phi_j = \Phi(z_j)$. The discrete equations become

$$s_T U_n + U_n\left(-\frac{1}{(\Delta z)} + \frac{\mathcal{P}}{2}\right) + \frac{U_{n-1}}{(\Delta z)} = 0, \tag{B.6}$$

$$s_T U_1 + U_1\left(\frac{1}{\Delta z} - \frac{\mathcal{P}}{2}\right) - \frac{U_2}{(\Delta z)} = 0, \tag{B.7}$$

$$\frac{\epsilon^2}{\mu}\left[(s_T^2 - \mathcal{P}^2/4 - k^2)\Phi_j - \mathcal{P}\frac{\Phi_{j+1} - \Phi_{j-1}}{2(\Delta z)}\right] - \frac{\epsilon^2}{(\Delta z)^2}(\Phi_{j+1} + \Phi_{j-1} - 2\Phi_j) +$$
$$\epsilon^2 k^2\Phi_j + \frac{p'''(\bar{\phi}_j)}{120}\Phi_j - \alpha\Delta\epsilon\left[p''(\bar{\phi}_j)\bar{u}_j\Phi_j + p'(\bar{\phi}_j)U_j\right], \tag{B.8}$$

$$(s_T^2 - \mathcal{P}^2/4)U_j - \frac{1}{(\Delta z)^2}(U_{j+1} + U_{j-1} - 2U_j) - \mathcal{P}\frac{U_{j+1} - U_{j-1}}{2(\Delta z)} +$$
$$\frac{1}{\Delta}\left[p'(\bar{\phi}_j)(s_T^2 - \mathcal{P}^2/4 - k^2)\Phi_j - \mathcal{P}p''(\bar{\phi}_j)\bar{\phi}_{zj}\Phi_j - \mathcal{P}p'(\bar{\phi}_j)\frac{\Phi_{j+1} - \Phi_{j-1}}{2(\Delta z)}\right] = 0. \tag{B.9}$$

Here we have $\Phi_2, ..., \Phi_{n-1}$ and $U_1, ..., U_n$ for a total of $2n - 2$ unknowns. We can define the vector

$$X = [\Phi_2, ..., \Phi_{n-1}, U_1, ..., U_n]^T, \tag{B.10}$$

23

where the superscript T denotes the transpose, and then the above equations may be written as

$$\left(s_T^2 P + s_T Q + R\right) X = 0, \tag{B.11}$$

where P, Q, R are matrices which are determined from Eqs. (B.6)-(B.9). The first two rows of P are zero, and the remaining submatrix we call $\hat{P}$. In Q, $Q(1, 2n-2) = Q(2, n-1) = 1$ and all the remaining elements are zero. Note that R is not tridiagonal.

As discussed in [39], we can rewrite the singular quadratic problem for s_T with the change of variable $Y = [X^T, s_T(\hat{P}X)^T]^T$ to put the equation in standard generalized eigenproblem form

$$AY = s_T BY, \tag{B.12}$$

where A and B are given by

$$B = \left(\begin{array}{cc|c} & & 0_{2\times 2n-4} \\ Q & & \\ & & I_{2n-4} \\ --- & & --- \\ \hat{P} & & 0_{2n-4} \end{array}\right) \tag{B.13}$$

$$A = \left(\begin{array}{c|c} -R & 0_{2n-2} \\ --- & --- \\ 0_{2n-4} & I_{2n-4} \end{array}\right). \tag{B.14}$$

This system may then be solved for its eigenvalues (s_T) and eigenvectors, and the largest eigenvalue and corresponding eigenvector are typically of interest. The advantage here is that the new system is easily solved with standard packages, while the price to be paid is that the system size is nearly doubled.

References

[1] J.S. Langer, in *Directions in Condensed Matter Physics*, edited by G. Grinstein and G. Mazenko, (World Scientific, Philadelphia, 1986), pp. 164-186.

[2] G. Caginalp, "Stefan and Hele-Shaw type models as asymptotic limits of the phase-field equations," *Phys. Rev. A* **39**, 5887 (1989).

[3] G. Caginalp and E.A. Socolovsky, "Computation of Sharp Phase Boundaries by Spreading: The Planar and Spherically Symmetric Cases," *J. Comp. Phys.* **95**, 85 (1991); "Efficient Computation of a Sharp Interface by Spreading via Phase Field Models," *Appl. Math. Lett.* **2**, 117 (1989).

[4] K.E. Brattkus, D.I. Meiron and B.J. Spencer, "The Dynamic Consistency of Diffuse Phase-Field Models," (1992, pending publication).

[5] R. Kobayashi, *Bull. Jpn. Soc. Ind. Appl. Math.* **1**, 22 (1991); "Modeling and numerical simulations of dendritic crystal growth," *Physica D* **63**, 410 (1993).

[6] A.A. Wheeler, B.T. Murray, and R.J. Schaefer, "Computation of Dendrites using a Phase-Field Model," *Physica D* **66**, 243 (1993).

[7] R. Kupferman, O. Shochet, E. Ben-Jacob and Z. Schuss, "Studies of a Phase-Field Model: Boundary Layer, Selected Velocity and Stability Spectrum," (1993, pending publication).

[8] O. Penrose and P.C. Fife, "Thermodynamically-Consistent models of phase-field type for the kinetics of phase transitions," *Physica D* **43**, 44 (1990).

[9] S-L. Wang, R.F. Sekerka, A.A. Wheeler, B.T. Murray, S.R. Coriell, R.J. Braun and G.B. McFadden, "Thermodynamically-Consistent Phase-Field Models for Solidification," *Physica D*, (1993, to appear).

[10] S.M. Allen and J.W. Cahn, "A Microscopic Theory for Antiphase Boundary Motion and Its Application to Antiphase Domain Coarsening," *Acta Metall. Mater.* **27**, 1085 (1979).

[11] P.L. Harowell and D.W. Oxtoby, "On the Interaction Between Order and a Moving Interface: Dynamical disordering and anisotropic growth rates," *J. Chem. Phys.* **86**, 2932 (1987).

[12] A.A. Wheeler, W.J. Boettinger, and G.B. McFadden, "Phase-Field Model for Isothermal Phase Transitions in Binary Alloys," *Phys. Rev. E* **47**, 1893 (1993).

[13] W.W. Mullins and R.F. Sekerka, "Morphological Stability of a Particle Growing by Diffusion or Heat Flow," *J. Appl. Phys.* **34**, 323 (1963); "Stability of a Planar Interface During Solidification of a Dilute Binary Alloy," *J. Appl. Phys.* **35**, 444 (1964).

[14] J. Zittartz, "Microscopic approach to interfacial structure in Ising-like ferromagnets," *Phys. Rev.* **154**, 529 (1967).

[15] A. Umantsev and G.B. Olson, "Modulation mechanism for first-order transformations with nonconserved order parameters," *Phys. Rev. A* **46**, R6132 (1992).

[16] M. R. Scott and H. A. Watts, "Computational solution of linear two-point boundary value problems via orthonormalization," *SIAM J. Numer. Anal.* **14**, 40 (1977); an implementation is available in the SLATEC Common Math Library, Package 181-CY001-00, Energy Science and Technology Software Center, P.O. Box 1020, Oak Ridge, TN. 37381.

[17] H.B. Keller, *Numerical solution of two point boundary value problems*, CBMS-NSF Regional Conference Series in Applied Mathematics, (SIAM, Philadelphia, PA, 1976), vol. 24.

[18] D. Gottlieb and S.A. Orszag, *Numerical Analysis of Spectral Methods: Theory and Applications*, CBMS-NSF Regional Conference Series in Applied Mathematics, (SIAM, Philadelphia, 1977).

[19] M.E. Glicksman and R.J. Schaefer, "Investigation of Solid-Liquid Interface Temperatures via Isenthalpic Solidification," *J. Crystal Growth* **1**, 297 (1967).

[20] J.H. Perepezko, "Crystallization of Undercooled Liquid Droplets," in *Rapid Solidification Processing: Principles and Technologies II*, Proceedings of the Second International Conference on Rapid Solidification Processing, March 23-26, 1980, (Claitor, Baton Rouge, 1980), pp. 56-67.

[21] D.E. Herlach, "Containerless Undercooling and Solidification of Pure Metals," *Ann. Rev. Mater. Sci.* **21**, 23 (1991).

[22] R. Trivedi and W. Kurz, "Morphological stability of a planar interface under rapid solidification conditions," *Acta metall.* **34**, 1663 (1986).

[23] M.L. Frankel, "On the Weakly Nonlinear Evolution of a Perturbed Planar Solid-Liquid Interface," *Physica* **27D**, 260 (1987).

[24] E.A. Brener and D.E. Temkin, "Dendritic Growth at Deep Undercooling and Transition to a Planar Front," *Europhys. Lett.* **10**, 171 (1989).

[25] C. Misbah, H. Müller-Krumbhaar, and D.E. Temkin, "Interface Structure at Large Supercooling," J. Phys. I **1**, 585 (1991).

[26] G. Caginalp and J. Chadam, "Stability of interfaces with velocity correction term," *Rocky Mtn. J. of Math.* **21**, 617 (1991).

[27] A. Umantsev and S.H. Davis, "Growth From a Hypercooled Melt Near Absolute Stability," *Phys. Rev. A* **45**, 7195 (1992).

[28] J.B. Collins and H. Levine, "Diffuse Interface Model of Diffusion-Limited Crystal Growth," *Phys. Rev. B* **31**, 6119 (1985).

[29] Schofield and D.W. Oxtoby, "Diffusion Disallowed Crystal Growth. I. Landau-Ginzburg Model," *J. Chem. Phys.* **94**, 2176 (1991).

[30] H. Löwen, Schofield and D.W. Oxtoby, "Diffusion Disallowed Crystal Growth. II. A Parabolic Model," *J. Chem. Phys.* **94**, 5685 (1991).

[31] H. Löwen, and J. Bechhoefer, "Critical Behavior of Crystal Growth Velocity," *Europhys. Lett.* **16**, 195 (1991).

[32] H. Löwen, J. Bechhoefer, and L.S. Tuckerman, "Crystal growth at long times: Critical behavior at the crossover from diffusion to kinetics-limited regimes," *Phys. Rev. A* **45**, 2399 (1992).

[33] A. Umantsev, "Thermodynamic stability of phases and transition kinetics under adiabatic conditions," *J. Chem. Phys.* **96**, 605 (1991).

[34] G. Bader and U. Ascher, "A New Basis Implementation for a Mixed Order Boundary Value ODE Solver," *SIAM J. Sci. Stat. Comput.* **8**, 483 (1987); U. Ascher, J. Christiansen and R.D. Russell, "Collocation Software for Boundary-Value ODEs," *ACM TOMS* **7**, 209 (1981).

[35] M.J.D. Powell, "A Hybrid Method for Nonlinear Equations," in "Numerical Methods for Nonlinear Algebraic Equations," edited by P. Rabinowitz, (Gordon and Breach, New York, 1970).

[36] L.F. Shampine and H.A. Watts, "FZERO, A Root-Solving Code," Sandia National Laboratory Report SC-TM-70-631, (1970).

[37] T.J. Dekker, "Finding a Zero by Means of Successive Linear Interpolation," in "Constructive Aspects of the Fundamental Theorem of Algebra," ed. B. Dejon and P. Henrici, (1969).

[38] R.J. Schaefer, M.E. Glicksman, and J.D. Ayers, "High-Confidence Measurement of Solid/Liquid Surface Energy in a Pure Material," *Philos. Mag.* **32**, 725 (1975).

[39] A.J. Pearlstein, and D.A. Goussis, "Efficient Transformation of Certain Singular Polynomial Matrix Eigenvalue Problems," *J. Comp. Phys.* **78**, 305 (1988).

[40] J.S. Langer, "Instabilities and Pattern Formation in Crystal Growth," *Rev. Mod. Phys.* **52**, 1 (1980).

[41] G.A. Colligan and B.J. Bayles, *Acta Metall.* **10**, 895 (1962).

[42] J. Guckenheimer and P. Holmes, "Nonlinear Oscillations, Dynamical Systems, and Bifurcations of Vector Fields," (Springer, Berlin, 1990), corrected 3rd edition, p. 364.

[43] A.A. Wheeler, W.J. Boettinger, and G.B. McFadden, "Phase-Field Model of Solute Trapping during Solidification," *Phys. Rev. E* **47**, 1893 (1993).

[44] C. Canuto, M.Y. Hussaini, A. Quarteroni, and T.A. Zang, *Spectral Methods in Fluid Mechanics*, (Springer, New York, 1988).

[45] D. Gottlieb, M.Y. Hussaini, and S.A. Orszag, in *Spectral Methods for Partial Differential Equations*, edited by G.R. Voigt, D. Gottlieb, and M.Y. Hussaini, (SIAM, Philadelphia, 1984) pp. 1-54.

ϵ	$\mathcal{P}$	Δ	k_0
0	1.5×10^{-3}	1.03	0.0270033
1.0	1.5559×10^{-3}	1.03	0.0275115
4.0	1.5×10^{-3}	1.02535	0.0272539

Table 1: Marginally-stable wavenumber k_0 for sharp-interface results ($\epsilon = 0$) compared two ways with phase-field results. In the second line, the bulk undercooling is held fixed. In the third line, the speed of the planar front is held fixed.
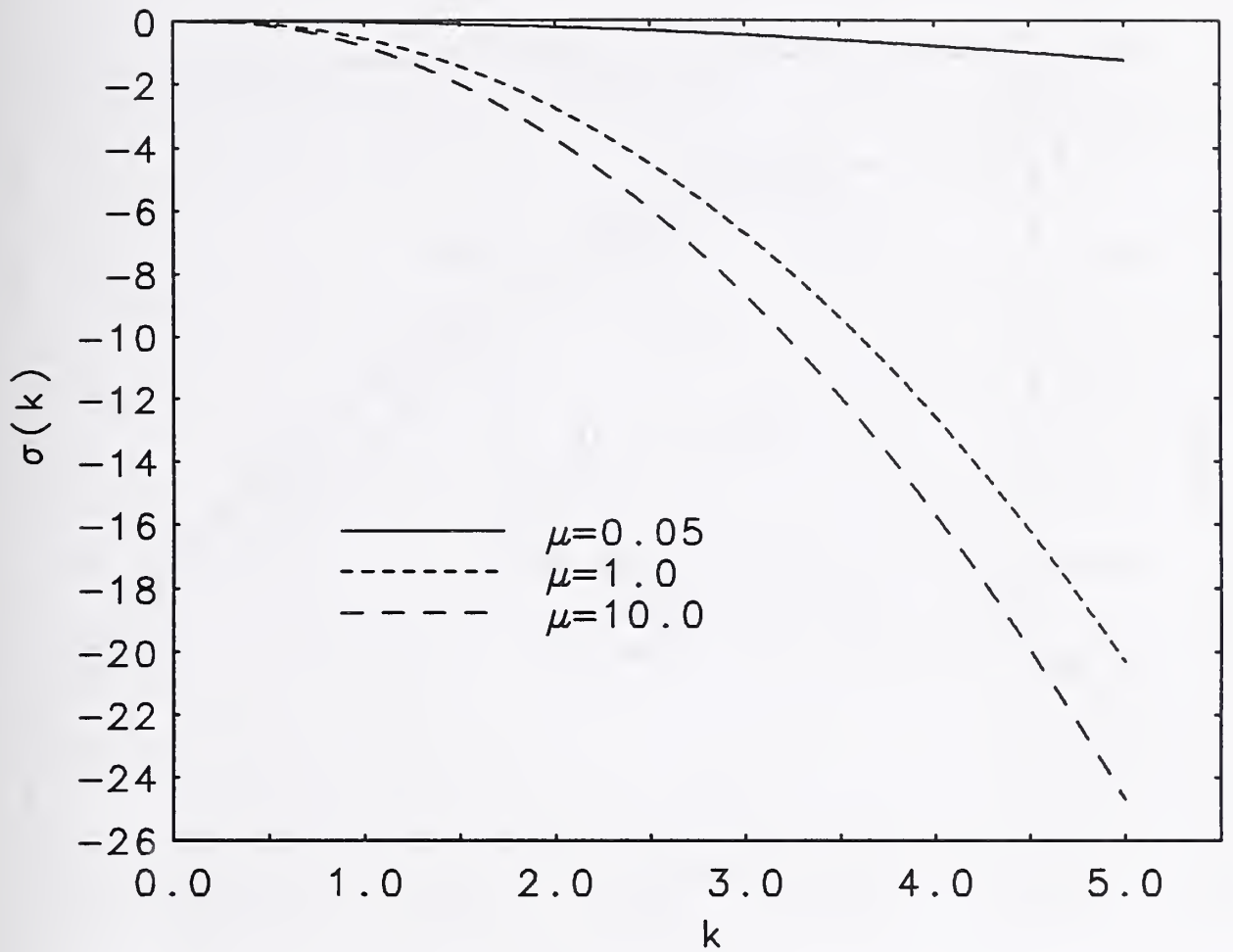
Figure 1: Sharp-interface linear-stability growth rates σ as a function of the wavenumber k are shown for several values of the attachment kinetics parameter μ. The results change imperceptibly from the $\mu = 10$ case for larger μ.
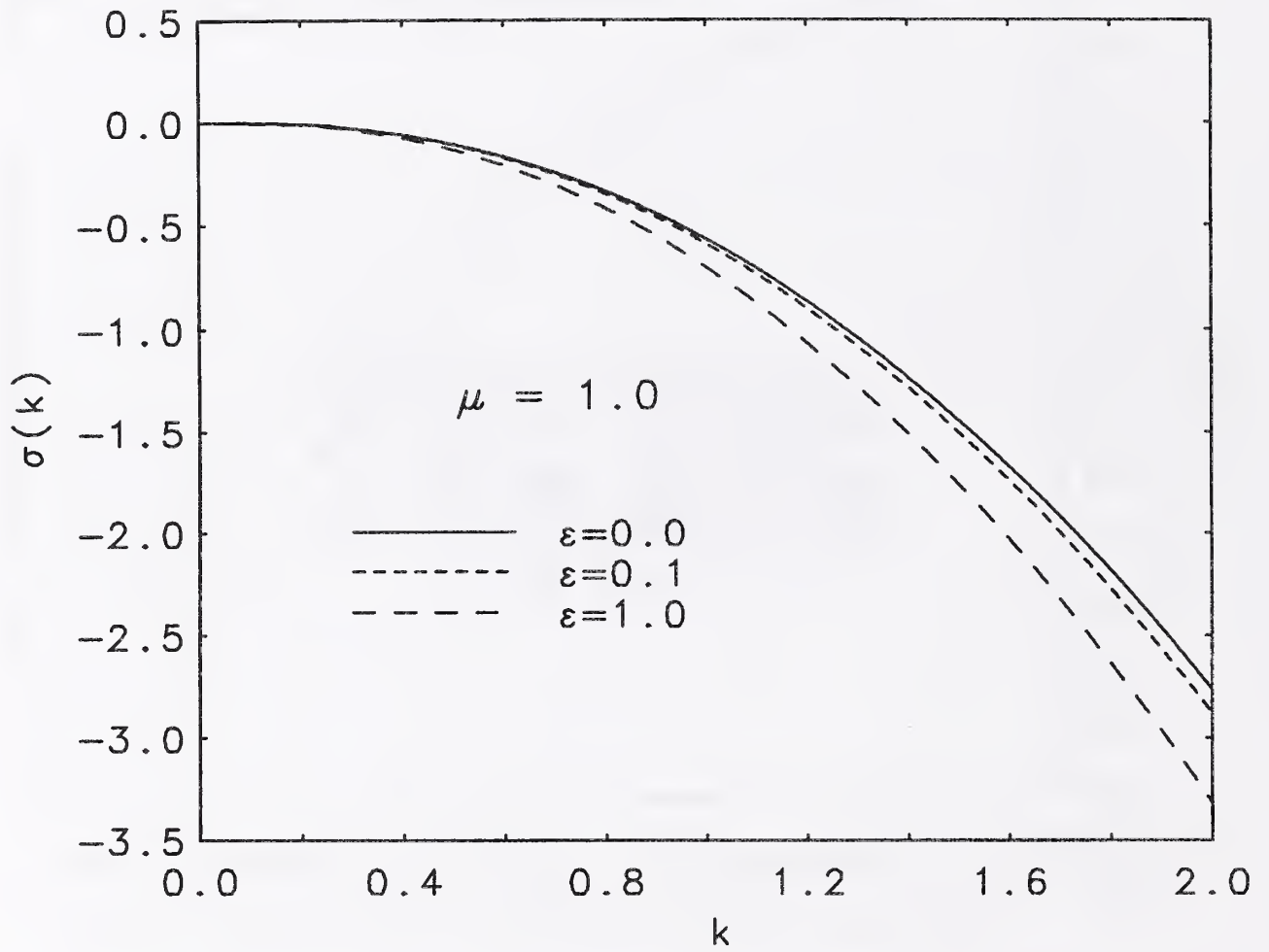
Figure 2: Linear theory growth rates for the isothermal planar front are shown for different values of the nondimensional thickness of the front ϵ. Here $\mu = 1$.
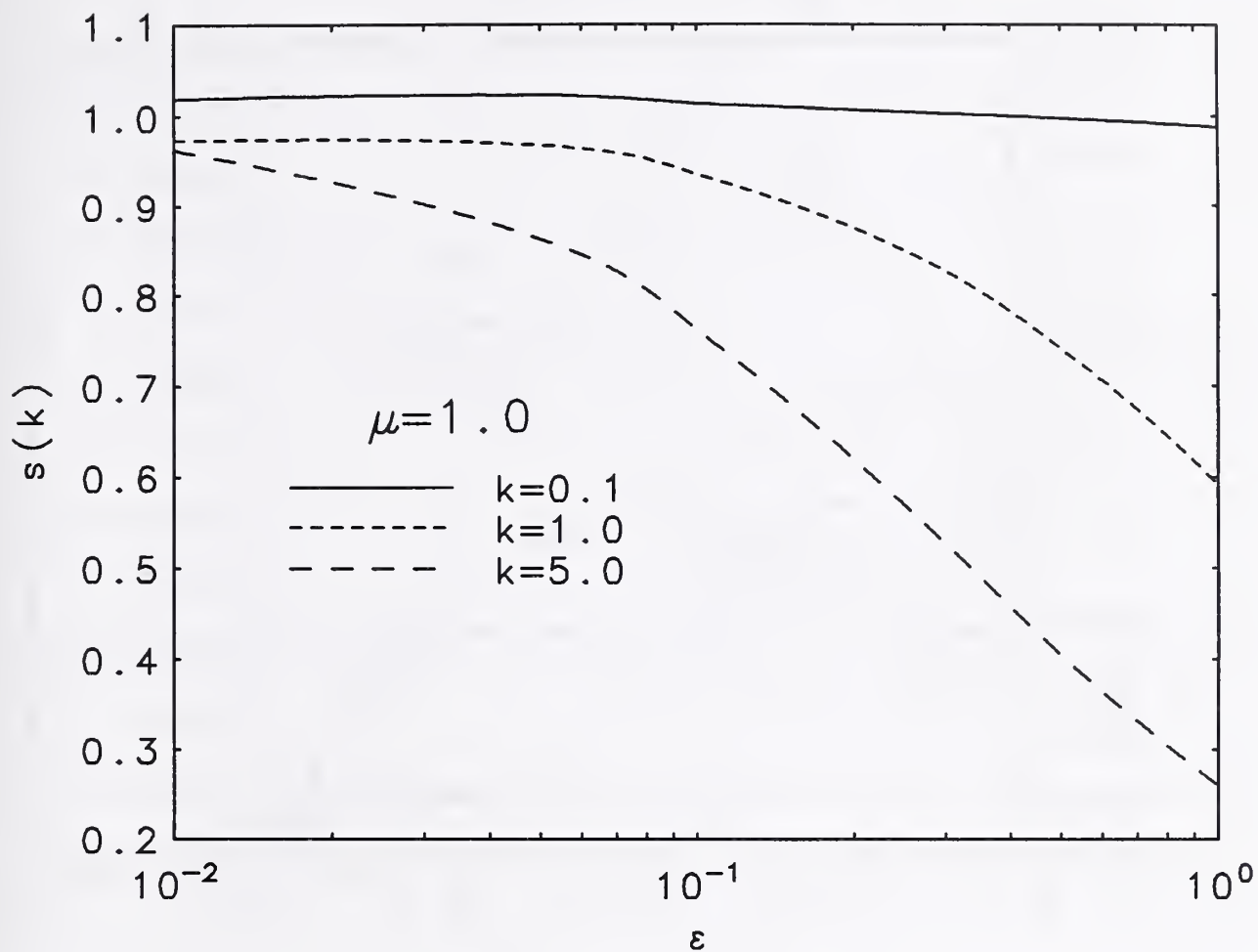
Figure 3: Convergence of the asymptotic results for the phase-field model to the sharp-interface stability results for the isothermal planar front as the interface thickness tends to zero, for various values of the wavenumber, k. The quantity $s(k)$ is defined by Eq. (2.29).

31
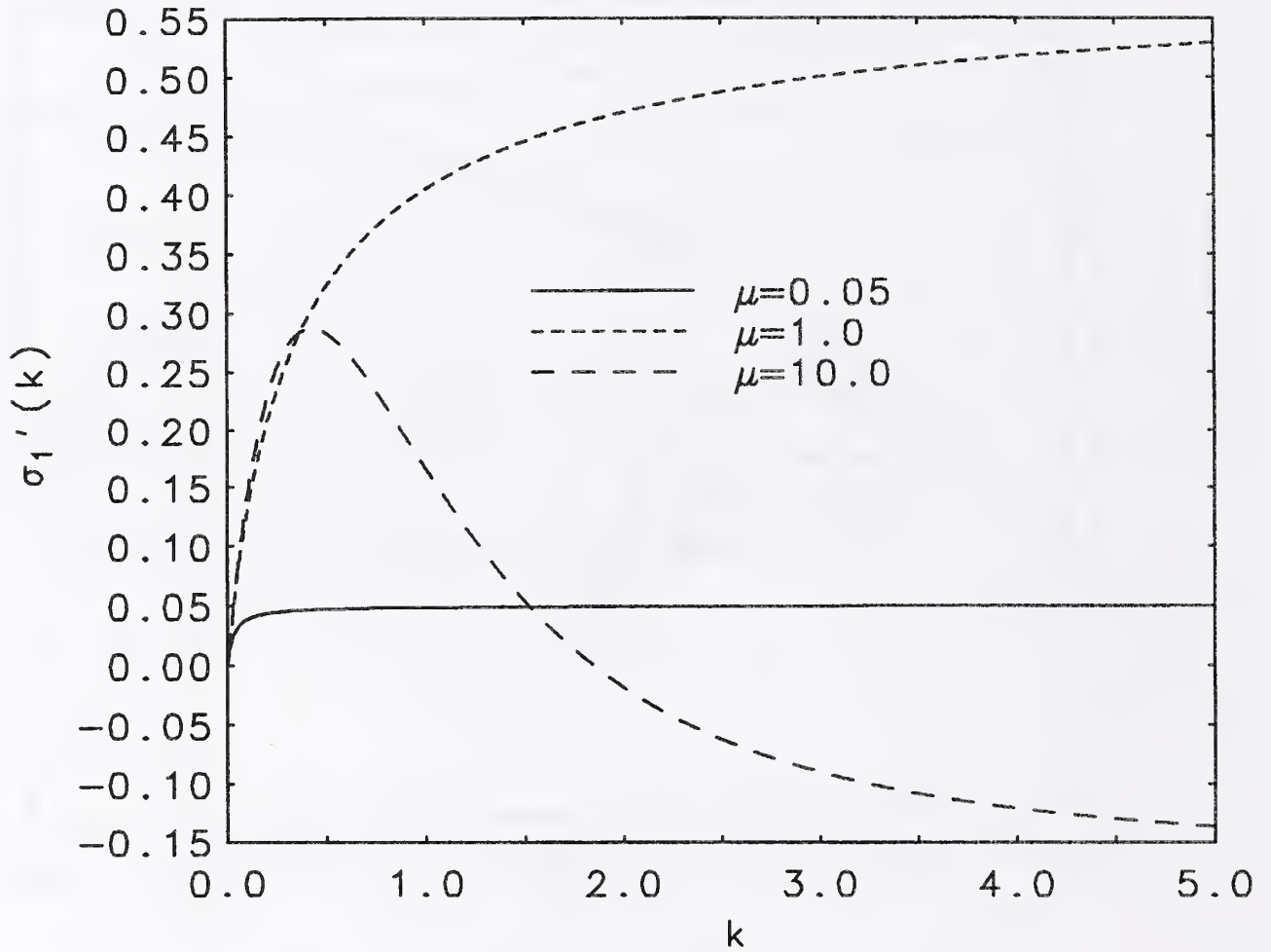
Figure 4: The correction to the sharp interface growth rate σ_1', given by Eq. (2.27), is shown as a function of the wavenumber k for several values of the nondimensional attachment kinetics parameter μ.
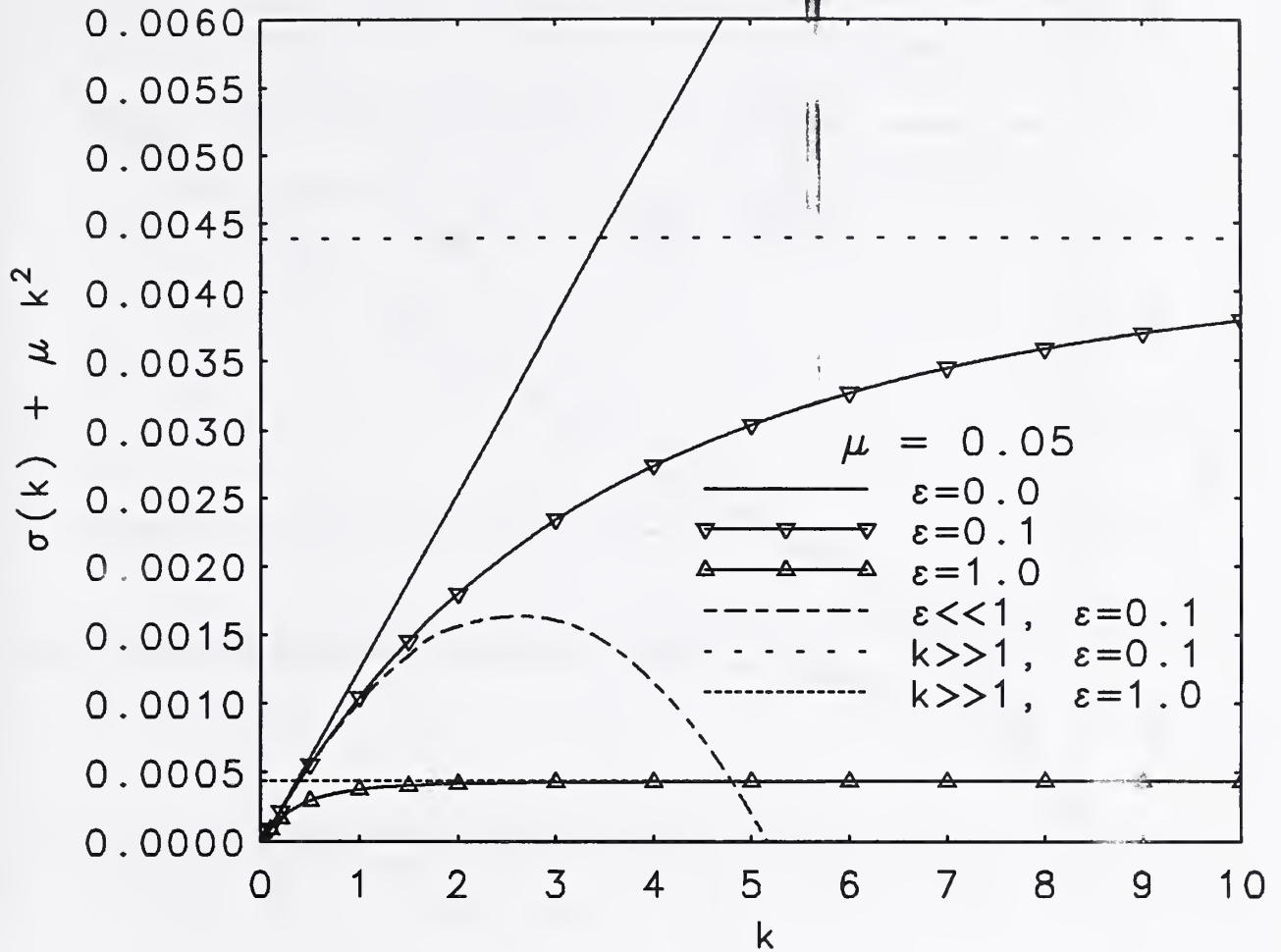
Figure 5: A comparison of numerical and asymptotic results for $\mu = 0.05$. The leading order behavior $(-\mu k^2)$ is subtracted off in order to emphasize the differences in behavior. The solid curve corresponding to $\epsilon = 0$ is the sharp interface result. The curves with triangles corresponding to finite ϵ approach the horizontal curves representing the $k \gg 1$ asymptotic results. The curve $\epsilon \ll 1$ is the asymptotic result in the limit $\epsilon \to 0$, k fixed, evaluated at $\epsilon = 0.1$.
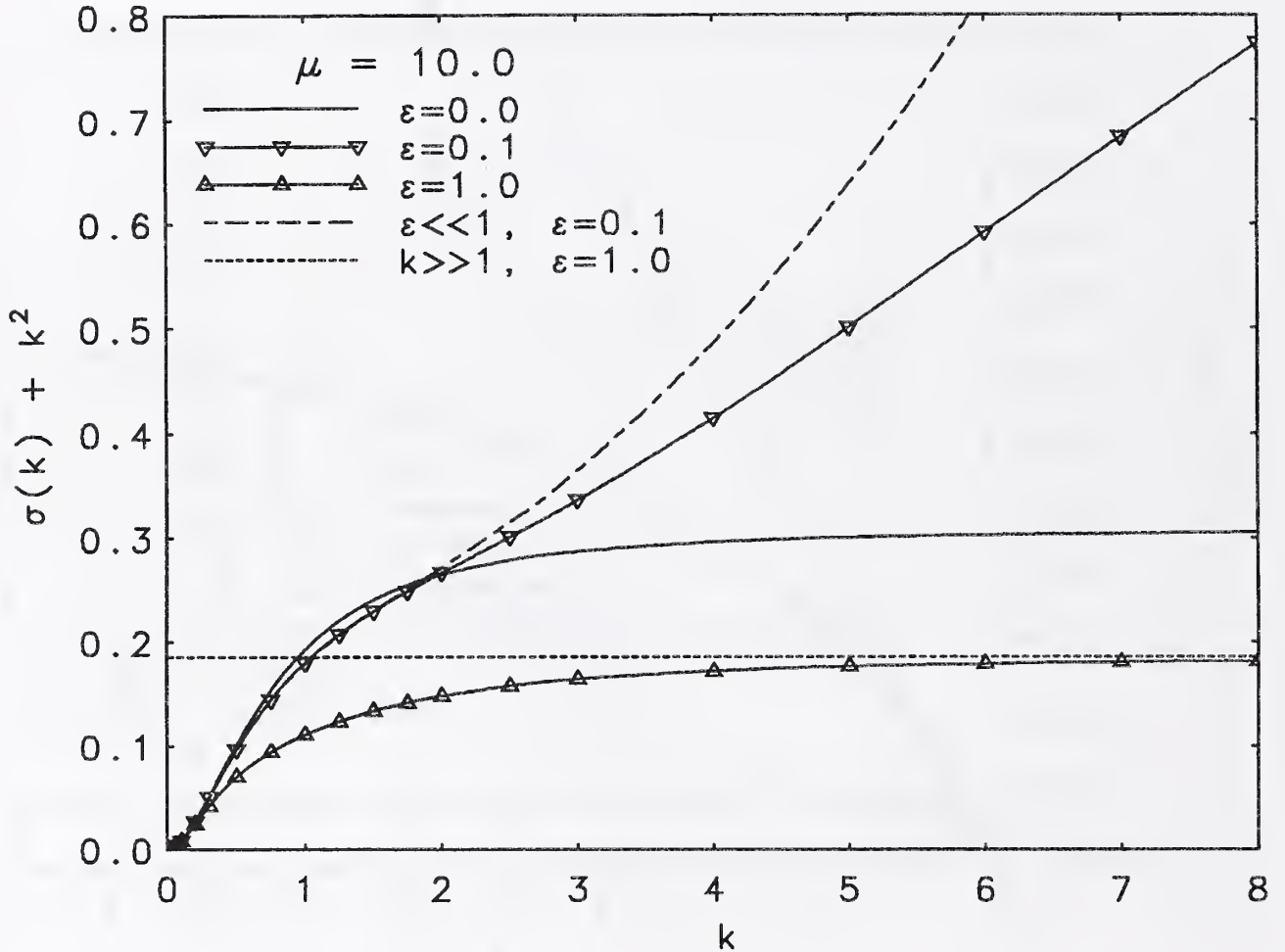
Figure 6: A comparison of numerical and asymptotic results for $\mu = 10$. The leading order behavior $(-k^2)$ is subtracted off in order to emphasize the differences in behavior. The solid curve corresponding to $\epsilon = 0$ is the sharp interface result. The curves with triangles corresponding to finite ϵ approach the horizontal curves representing the $k \gg 1$ asymptotic results. The curve $\epsilon \ll 1$ is the asymptotic result in the limit $\epsilon \to 0$, k fixed, evaluated at $\epsilon = 0.1$. The numerical solution for $\epsilon = 0.1$ approaches a constant value that is not shown on the graph for larger values of k.
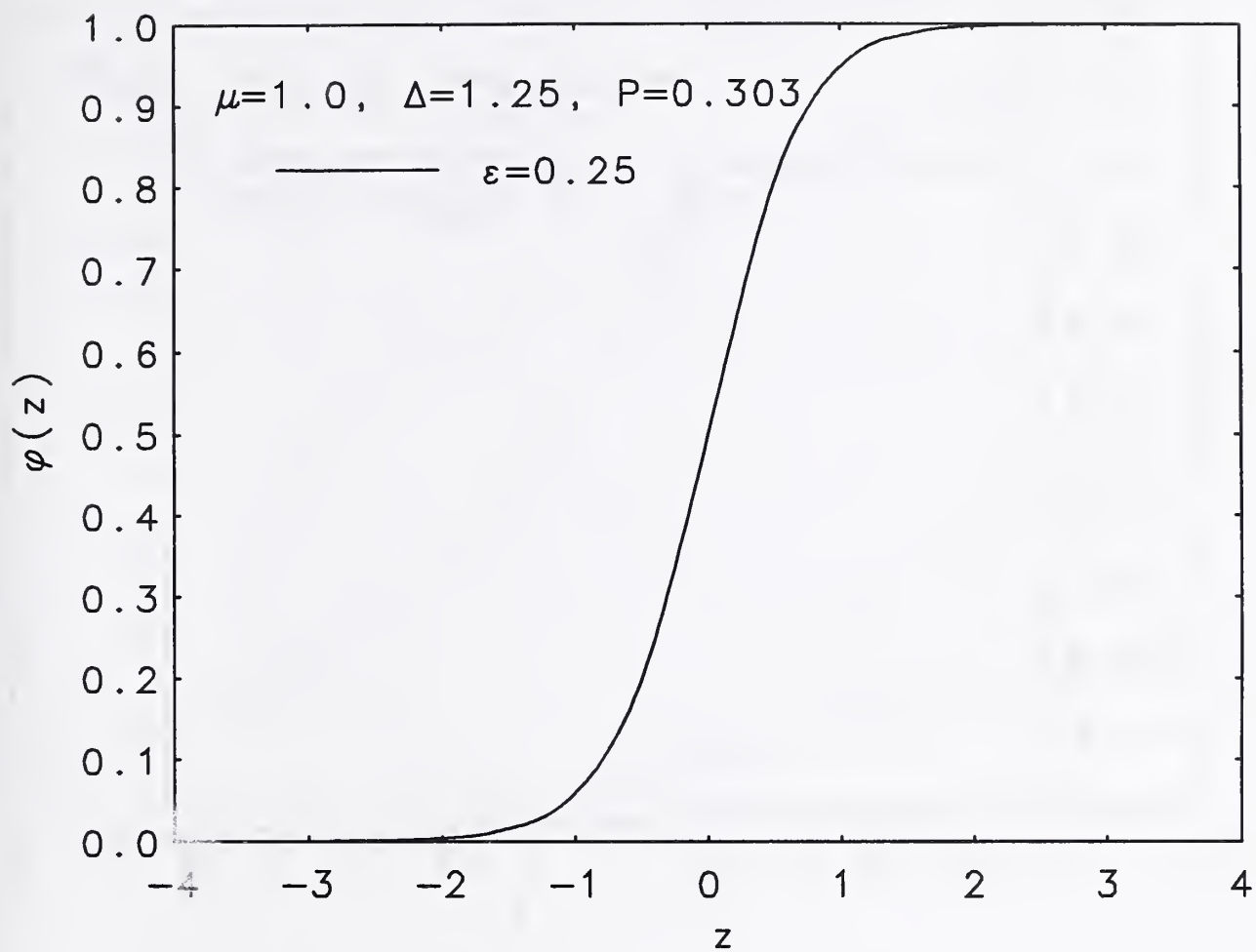
Figure 7: Computed base states showing phase field $\bar{\phi}(z)$ as a function of the spatial variable z.
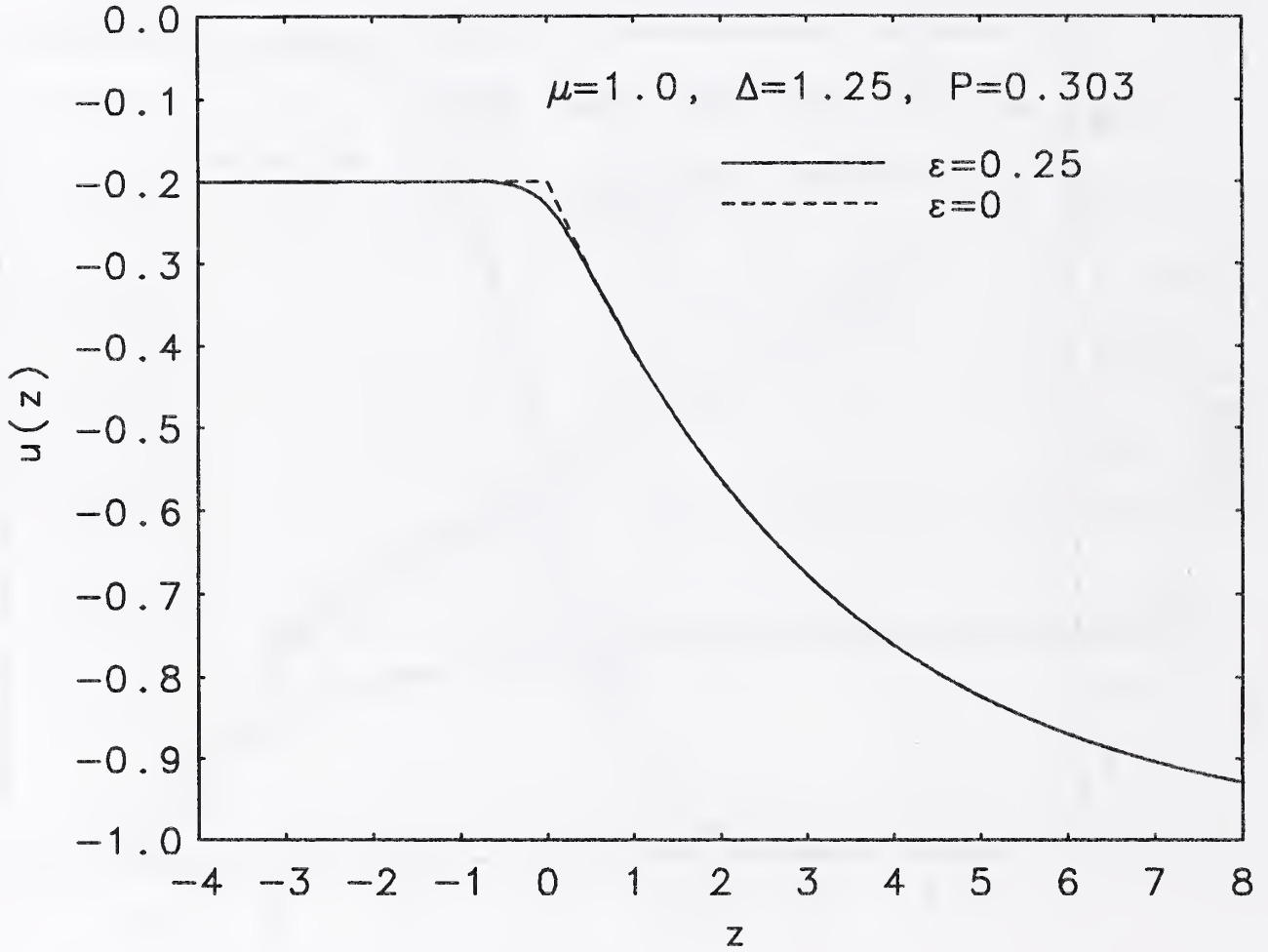
Figure 8: Computed base states showing the temperature field $\bar{u}(z)$ as a function of the spatial variable z. The phase field result in the solid curve; the dashed curve is the sharp interface result.
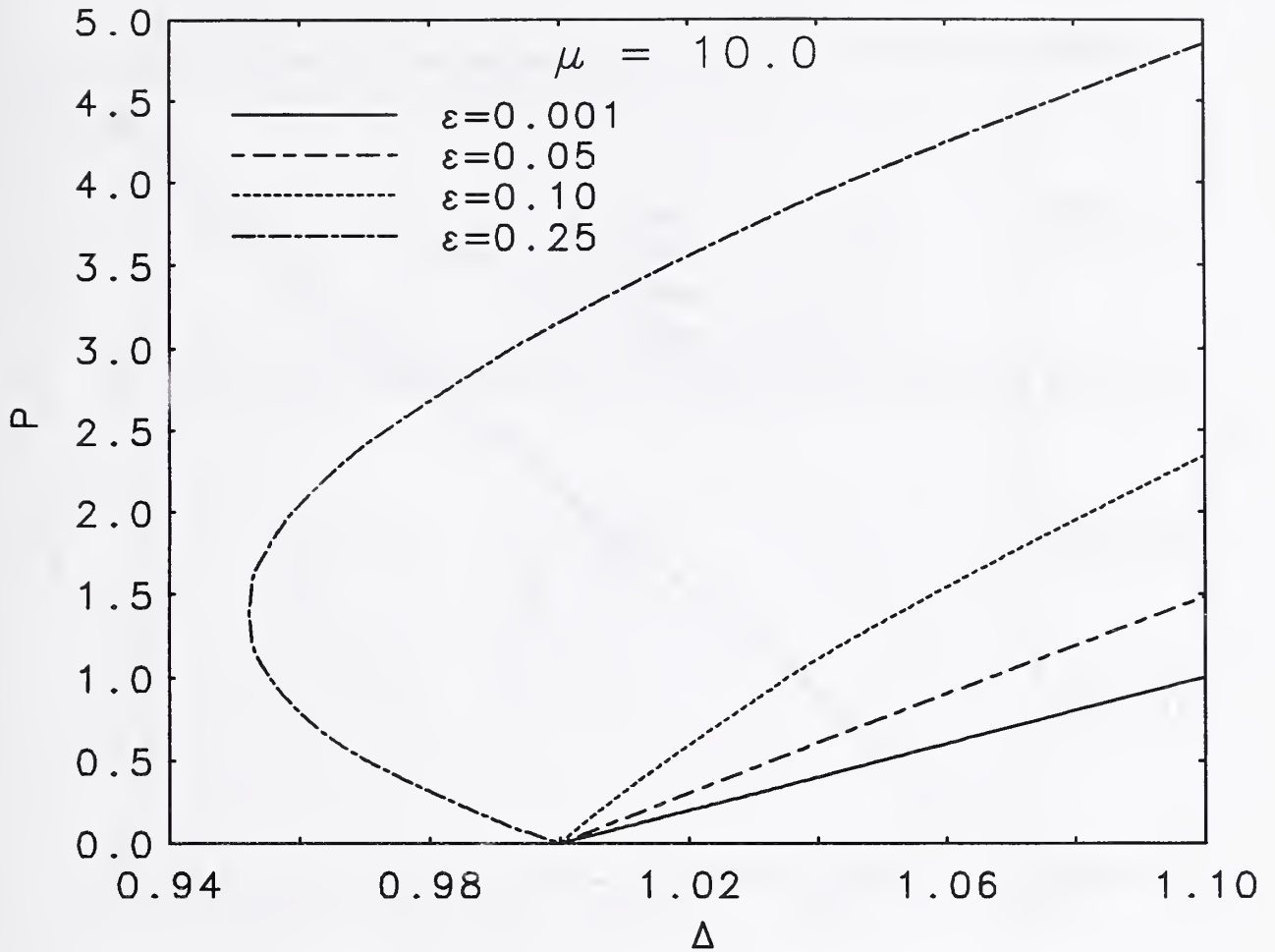
Figure 9: Computed base states for several values of the nondimensional interface thickness ϵ for $\mu = 10.0$; for this high rate of attachment and sufficiently large ϵ, the model we use displays constant-speed growth for sub-unit undercoolings as seen in other phase field models [29–33].
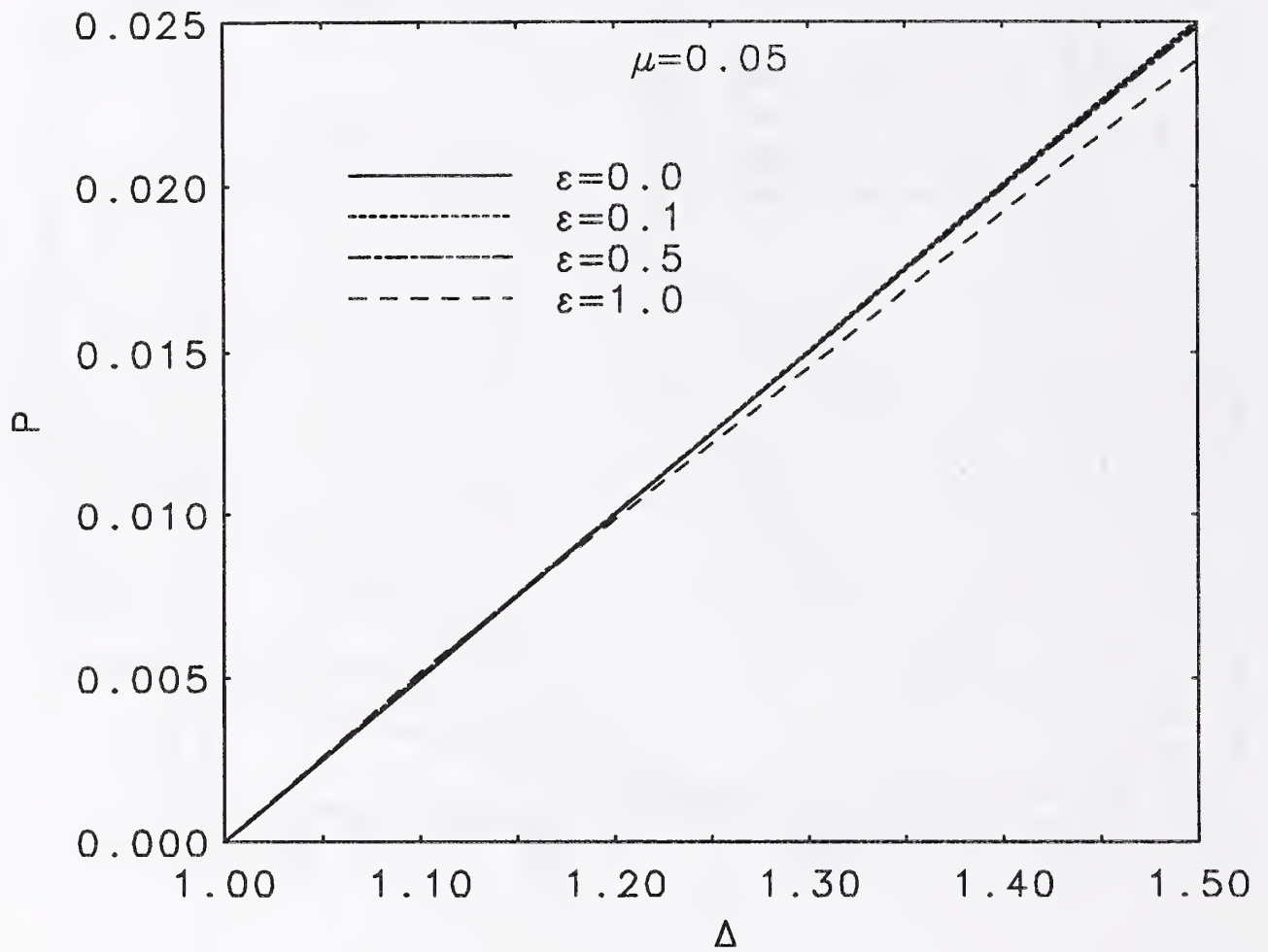
Figure 10: Computed base states for several values of the nondimensional interface thickness ϵ for $\mu = 0.05$.
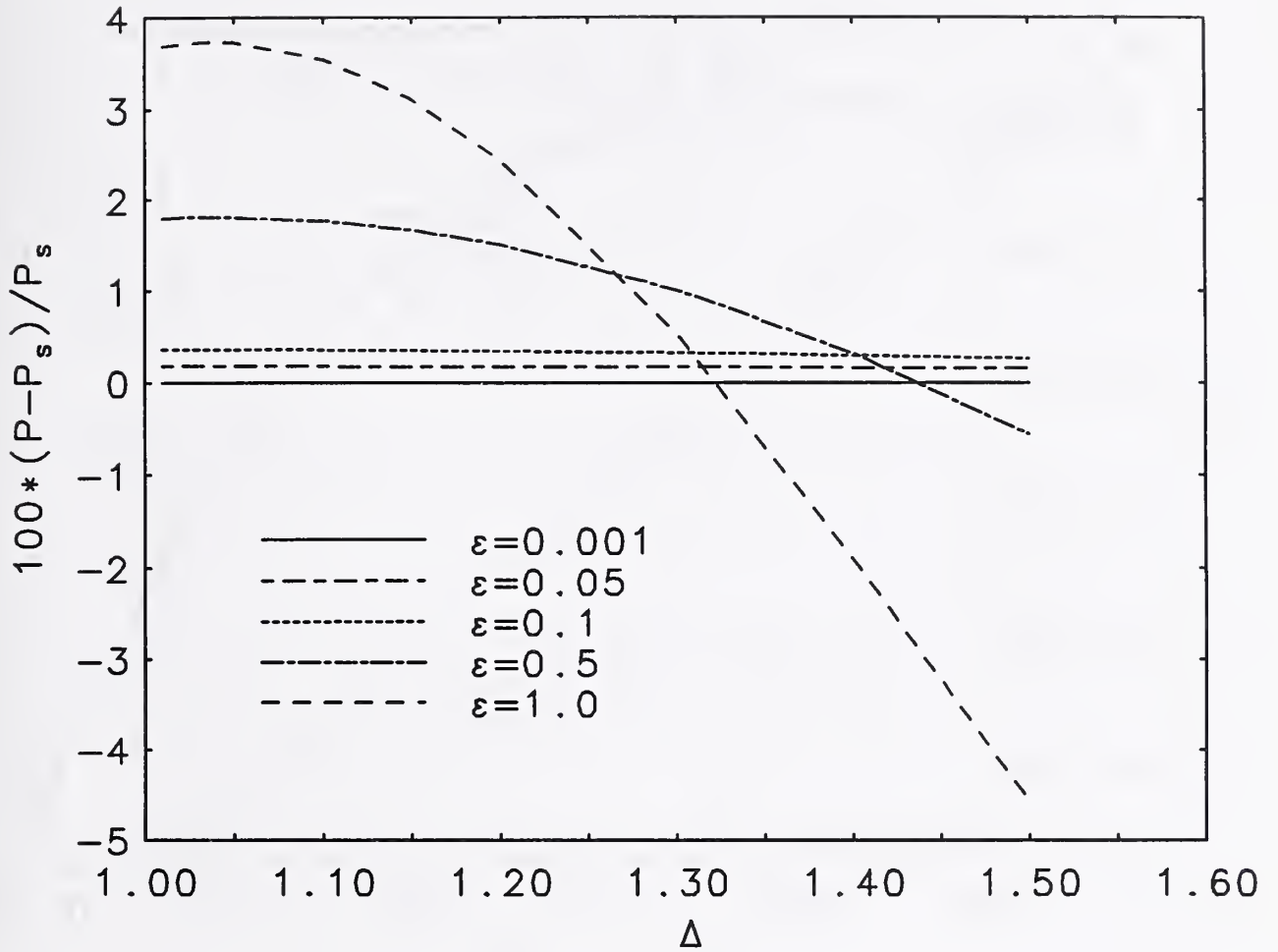
Figure 11: Deviation from the sharp interface base states for several values of the nondimensional interface thickness ϵ for $\mu = 0.05$. The speed of the front is reduced if the thickness of the front and the undercooling are large. Here P_S is the sharp interface front speed given by $P_S = \mu(\Delta - 1)$.
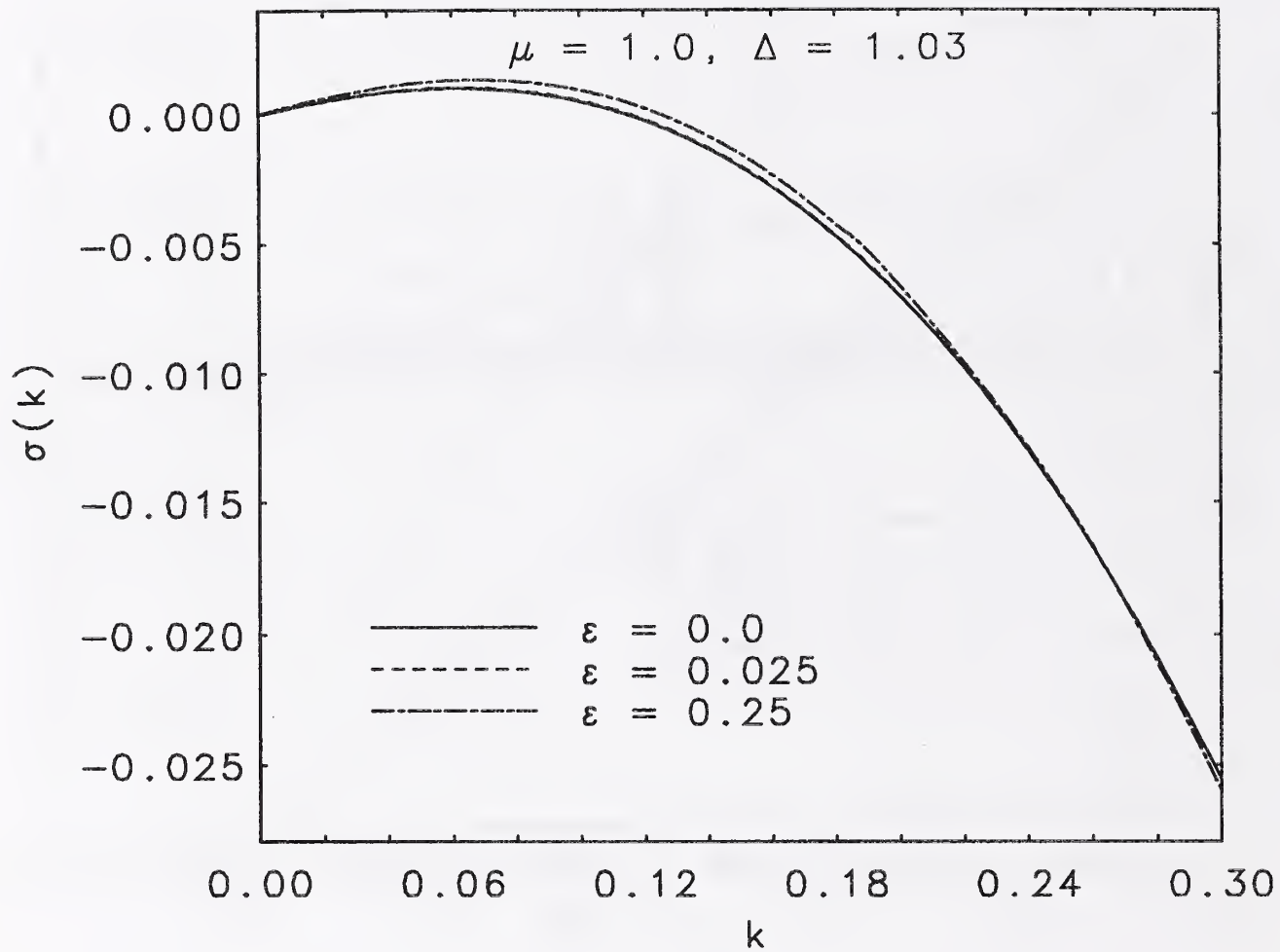
Figure 12: Growth rates σ as function of wavenumber k for sharp interface and phase-field models. The curve for $\epsilon = 0$ is the sharp-interface result; the curves for $\epsilon = 0$ and $\epsilon = 0.025$ are practically indistinguishable.
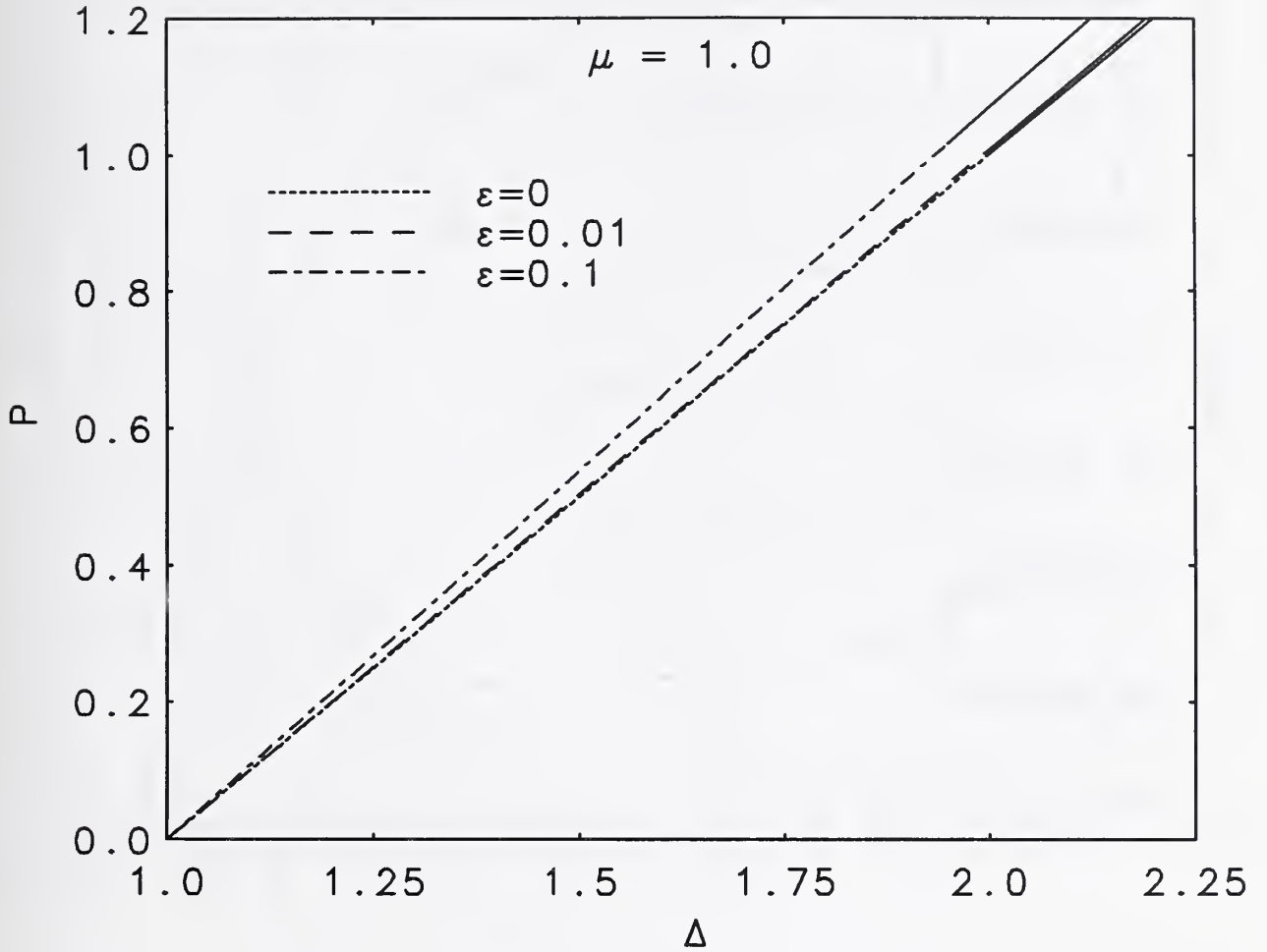
Figure 13: Stable and unstable regimes in sharp-interface ($\epsilon = 0$) and phase-field models ($\epsilon \neq 0$). The dashed (solid) curves denote unstable (stable) planar fronts. The curves for $\epsilon = 0$ and $\epsilon = 0.01$ are nearly indistinguishable.
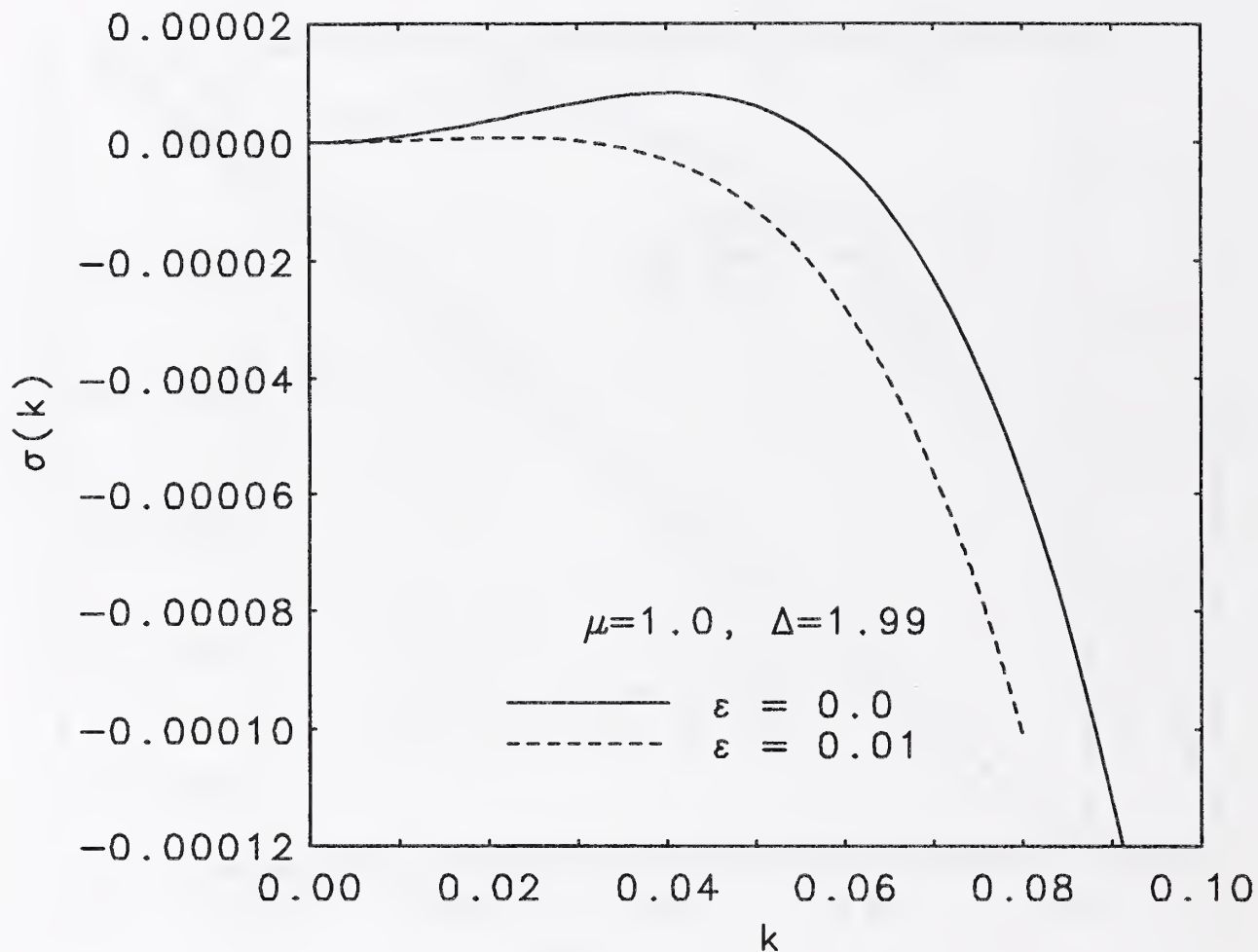
Figure 14: Growth rates σ as a function of wavenumber k near absolute stability. Increasing the undercooling to $\Delta = 1.995$ stabilized the planar front in the phase-field model; the undercooling must be larger than $\Delta = 2.0$ to stabilize the planar front in the sharp interface model.
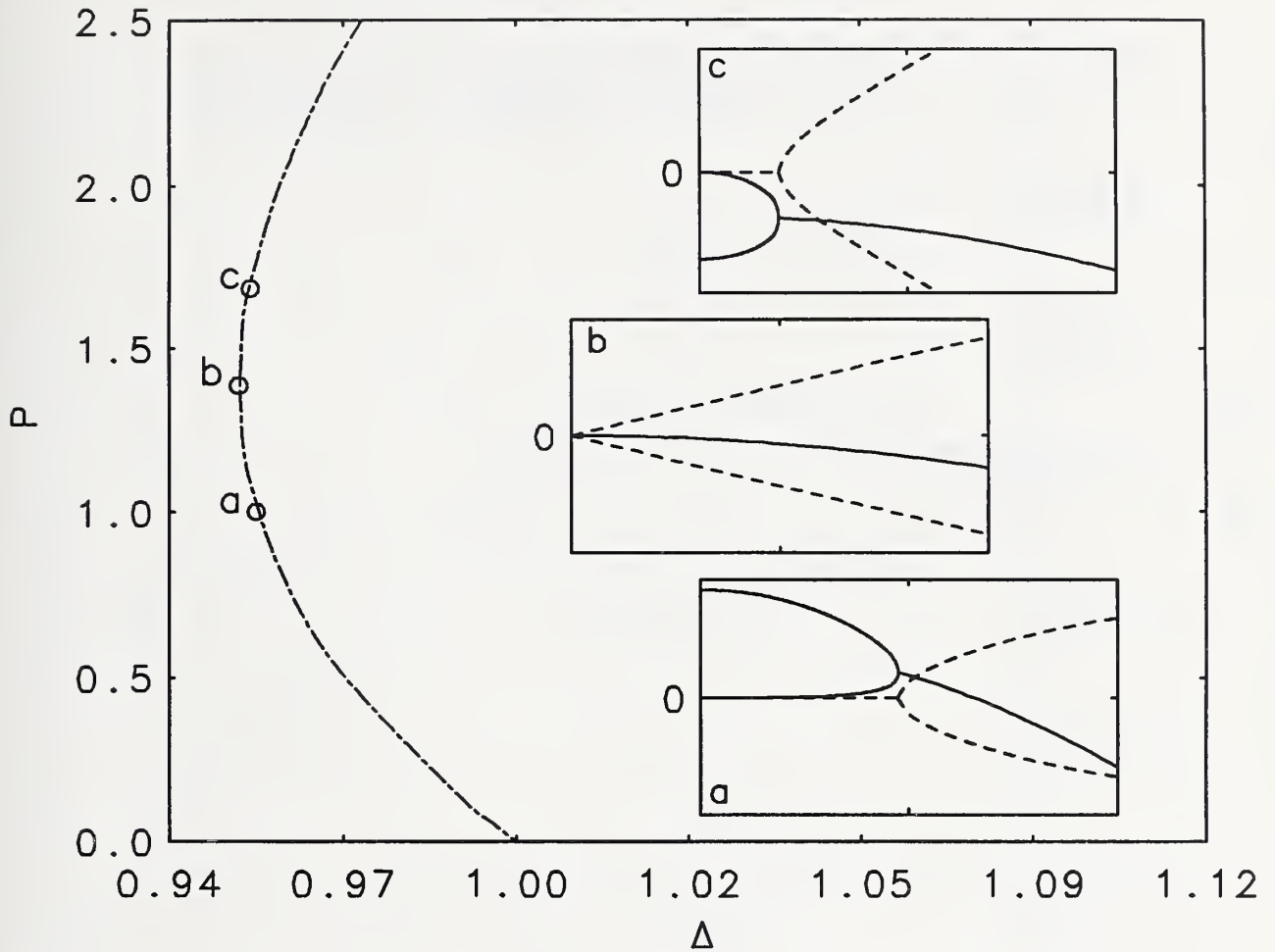
Figure 15: The stability results for $\mu = 10$ and $\epsilon = 0.25$ for the three indicated conditions; the curve on the left represents the planar front. Each inset figure is the corresponding plot of the growth rate σ vs. wavenumber k for those conditions; the range of the horizontal axes is $0 \leq k \leq 0.11$ in each case. The real (imaginary) part of the growth rate, σ_r (σ_i), is given by the solid (dashed) curve. The conditions for the three insets are: (a) $\mathcal{P} = 1.001$, $\Delta = 0.955$, $|\sigma_r, \sigma_i| < 0.2$; (b) $\mathcal{P} = 1.386$, $\Delta = 0.952$, $|\sigma_r, \sigma_i| < 0.1$; (c) $\mathcal{P} = 1.686$, $\Delta = 0.954$, $|\sigma_r, \sigma_i| < 0.07$.
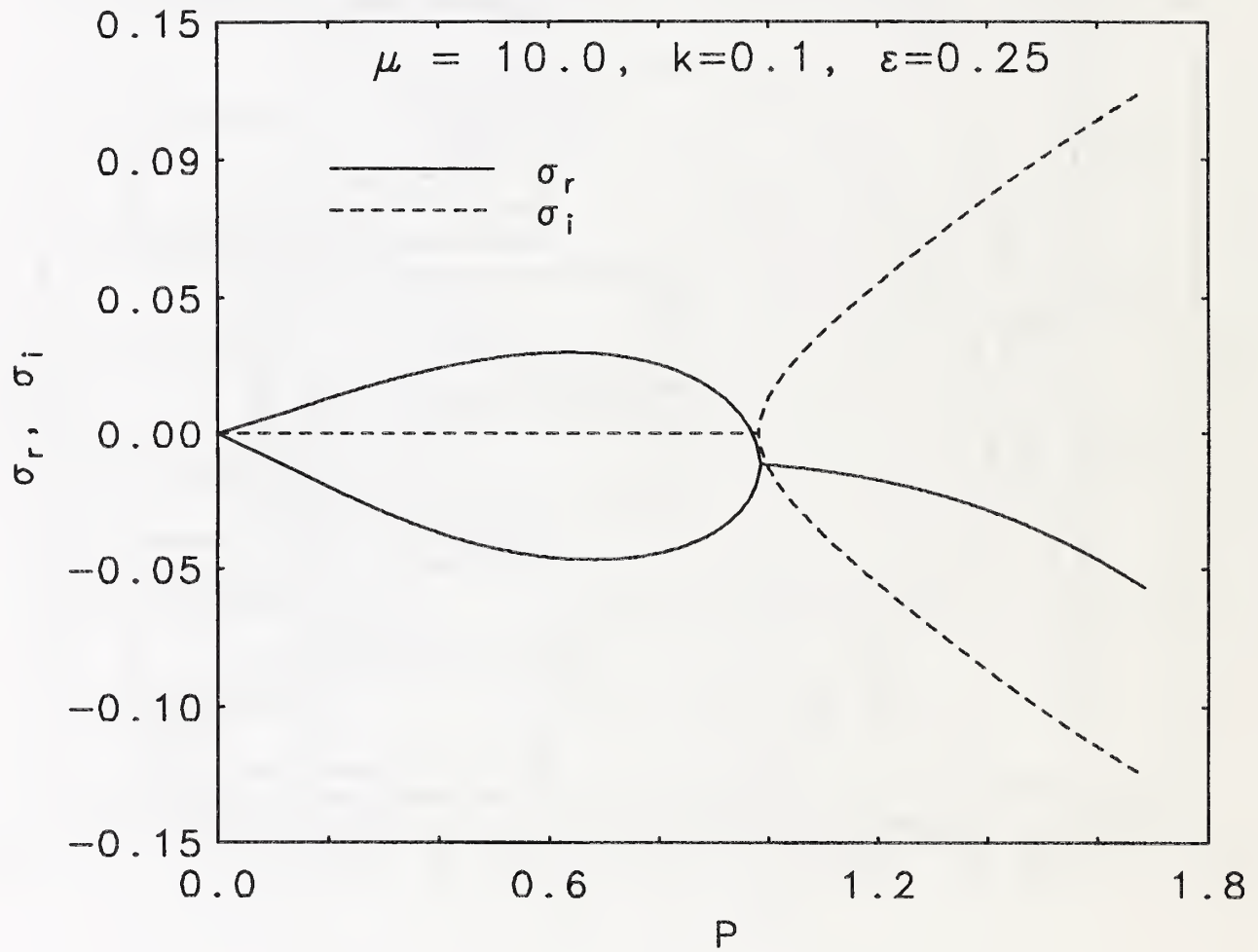
Figure 16: The growth rates σ of the first two modes are plotted against the nondimensional growth speed $\mathcal{P}$ for fixed $k = 0.1$. The real part σ_r is the solid curve and the dashed curves are the imaginary parts σ_i.